Computational fluid dynamics simulations of ship airwake

N Sezer-Uzol, A Sharma, and **L N Long***
Department of Aerospace Engineering, Pennsylvania State University, Pennsylvania, USA

The manuscript was received on 17 March 2005 and was accepted after revision for publication on 26 August 2005.

DOI: 10.1243/095441005X30306

Abstract: Computational fluid dynamics (CFD) simulations of ship airwakes are discussed in this article. CFD is used to simulate the airwakes of landing helicopter assault (LHA) and landing platform dock-17 (LPD-17) classes of ships. The focus is on capturing the massively separated flow from sharp edges of blunt bodies, while ignoring the viscous effects. A parallel, finite-volume flow solver is used with unstructured grids on full-scale ship models for the CFD calculations. Both steady-state and time-accurate results are presented for a wind speed of 15.43 m/s (30 knot) and for six different wind-over-deck angles. The article also reviews other computational and experimental ship airwake research.

Keywords: ship airwake, computational fluid dynamics, landing helicopter assault (LHA), landing platform dock-17 (LPD-17), dynamic interface, blade sailing

1 INTRODUCTION

Helicopter shipboard operations present a multitude of challenges. One of the primary factors that make it extremely difficult, and potentially dangerous, to perform helicopter flights to and from a ship deck is the unsteady ship airwake. Other factors that are also important are the possibly adverse weather and sea conditions, ship translation and rotation (oscillating landing spot), small flight decks (for some ships), and poor visibility conditions.

The most challenging rotorcraft/ship dynamic interface (DI) problems occur during:

(a) engagement and disengagement (run-up and run-down) of the rotor system while the aircraft is on the flight deck (i.e. the blade-sailing phenomena);
(b) takeoff and landing operations (e.g. launch, departure, approach and recovery);
(c) hovering over the moving flight deck (i.e. station-keeping).

It requires tremendous practice and skill for the pilots to learn to perform these operations. A common practice to ensure safe operation of helicopters from a ship is to find the safe helicopter operating limits (SHOLs) for a ship/helicopter combination. These are usually defined in terms of allowable wind conditions (direction and speed) over the deck and are called wind-over-the deck (WOD) envelopes.

It is difficult to obtain these WOD envelopes using real, full-scale experiments for a variety of reasons. A series of DI flight tests for all possible combinations of wind speed and azimuth (typically in 5 knot, 15° increments) must be performed to establish the envelope. However, these tests are costly, often limited (due to the absence of certain wind conditions and the availability of fleet assets), and unsafe. This process also depends on subjective pilot ratings. In contrast, scale model wind tunnel tests allow control over the wind conditions and can supply detailed information but are still costly and time consuming. In wind tunnel testing, small size ships (with lower Reynolds number) are used and the full-scale (high) Reynolds number cannot be obtained. In addition, the complexity of the flow field of a rotorcraft during takeoff and landing is impossible to reproduce in a wind tunnel. Furthermore, it is both difficult and costly to obtain high quality and complete sets of coupled ship airwake/rotorcraft flow field measurements using both full-scale and scaled-model tests for all of the different WOD conditions for any ship/helicopter

*Corresponding author: Department of Aerospace Engineering, Pennsylvania State University, University Park, PA 16802, USA.

combination that could be used to obtain the SHOLs.

A numerical procedure to analyse shipboard operations and to obtain the WOD envelope would be desirable because it is controlled, safer, and cheaper. It could also be used to train pilots by coupling with a flight simulator (as a piloted training tool). It can also be valuable as a non-real-time simulation tool for use in engineering and design by helping in the development of advanced flight control systems and in the design processes of future ships. Such numerical simulation tools could include:

(a) CFD simulations of the unsteady ship airwake;
(b) a high-fidelity flight dynamics model for the helicopter;
(c) a model for the ship motion;
(d) a model of a human pilot for analysing the pilot workload and response.

Understanding and modelling the airwake of a complex ship geometry present a number of technical challenges. The modelling requires an accurate representation of the complex ship geometry with superstructures and sharp edges. The flow around complex ship superstructures, including towers, antennae, radar dishes, exhaust stacks, and so on, is very difficult to predict. In addition, modelling of a moving flight deck because of ship translational speed and random sea motion must be taken into consideration. The effects of the atmospheric environment (atmospheric boundary layer and turbulence) and high winds are important. The ship airwake is also largely affected by the helicopter rotor and fuselage wakes and vice versa, resulting in complex interactions.

The ship airwake flow is highly three-dimensional, unsteady, separated, vortical, and turbulent. There are massive regions of flow separation and there is shedding of strong turbulent coherent structures from the ship's superstructure and sharp edges. As a result, the ship airwake contains a wide range of spatial and temporal scales and large, unsteady vortical regions around and behind the superstructure and over the flight deck, which affect the rotor response, fuselage loads, and pilot workload. Therefore, turbulence modelling is also important for such simulations. It is a low Mach number flow; however, there are complex interactions with the complex helicopter rotor flow during shipboard operations. Hence, accurate modelling and prediction of the highly unsteady airwake of a ship is critical for shipboard operations of rotorcrafts. To accurately resolve all the flow features: turbulence, boundary layer, flow separation, and interaction of helicopter flow-field with the ship airwake, in a time-accurate simulation is a big challenge. The magnitude of the unsteadiness demands long-time records which, coupled with large grids associated with such geometries, require enormous computational power. Full-scale or wind tunnel experiments, in contrast, can easily generate long-time records of data, but the associated initial set-up cost and time can be huge.

In this article, the use of CFD to simulate the ship airwake of two different classes of ships: the landing helicopter assault (LHA) and the landing platform dock (LPD)-17 is discussed. A comprehensive study of the effect of WOD angle on the airwake is performed. Time accurate runs are performed for WOD angles of 0°, 30°, 45°, 90°, 270°, and 315°. The time-averaged solutions are analysed to investigate the characteristics of the wake. The simulations are performed using a uniform steady freestream with a wind speed of 15.43 m/s (30 knot). Although the effects of atmospheric boundary layer and atmospheric turbulence are important, they are not included in this article due to the computational time available, but these effects will be included in future simulations. Long-time histories (for a period of $\sim$40 s) are obtained for the WOD angles of 0° and 30° to determine dominant shedding frequencies for both ships. The unsteady nature of the wake is highlighted and a quantitative measure of the unsteadiness is presented. Because the simulations are performed without using any traditional turbulence model, the smallest turbulent scales that are captured in these simulations are of the order of the grid size. The flow is assumed to be inviscid in these simulations and hence the simulations do not capture boundary layer effects. It is prohibitively expensive to do time-accurate simulations for a grid that can resolve the boundary layer. The sharp edges of the ships' boundaries and the superstructures fix the separation points of the flow making it reasonably independent of the Reynolds number. Therefore, the inviscid flow approximation can be used for these simulations. Some results from these simulations have previously been successfully interfaced [**1**–**3**] with flight dynamics simulations to estimate pilot workload due to complex unsteady airwake.

In the following sections, the computational and experimental ship airwake research is reviewed in detail. A short review of the literature on the blade-sailing problem and DI simulations is also presented. In section 2, the ship airwake CFD simulations of the LHA and LPD-17 are described. The results of these simulations and the conclusions are presented in sections 3 and 4, respectively.

1.1 Previous ship airwake studies

Understanding and modelling the unsteady, separated, and turbulent airwakes of different classes of

ships have been the focus of numerous experimental and computational studies [**4**].

Experimental investigations include full-scale tests aboard ships such as LHA [**5**–**7**], as well as wind tunnel scaled-model tests, e.g. LHA [**6**–**8**], DD-963 [**9**, **10**], a non-aviation ship model [**11**–**13**], LPD-17 [**14**, **15**], a generic frigate [**16**], a Canadian patrol frigate (CPF) [**17**, **18**], a simple frigate shape (SFS) [**19**, **20**], a La Fayette frigate model [**21**], and others [**22**]. In addition to the ship airwake investigations, there have been several full-scale helicopter/ship DI experiments, e.g. XP-15 tiltrotor aboard landing platform helicopter (LPH)-class USS TRIPOLI [**23**], H-46 aboard USS GUAM (LPH-9) [**24**], and others [**25**]. Recently, wind tunnel tests to study the ship/helicopter interactions were also conducted [**26**–**28**]. Zan [**26**] investigated the effects of the wind speed and direction on rotor thrust of a four-bladed rotor model immersed in a CPF ship airwake. It was shown that the reduced inflow due to the ship airwake can significantly decrease the rotor thrust, therefore impacting the pilot workload and operational envelopes. Lee and Zan [**27**] performed wind tunnel experiments to investigate the unsteady aerodynamic loading on a rotorless Sea King fuselage in the turbulent airwake of a CPF ship. Silva *et al.* [**28**, **29**] obtained the V-22 tiltrotor airframe force and moment and detailed velocity field measurements operating over a scaled-model LHA ship.

Computational simulations of ship airwakes provide an attractive alternative and have been performed using different numerical approaches for different ships and WOD conditions. The steady-state Reynolds-averaged Navier–Stokes (RANS) simulations of an airwake were performed using unstructured grids for an LPD ship by Tai [**14**], for a DD-963 class ship by Tai and Carico [**30**], for a landing helicopter deck (LHD) ship using a enhanced grid by Tai [**31**], and using structured grids for an SFS by Reddy *et al.* [**32**], and also using hybrid grids for a surface effect ship by Moctar and Bertram [**33**]. Syms [**18**] explained that the differences between the steady RANS simulations and experimental data might be due to the unsteadiness in the flow, which cannot be handled by such simulations. In addition, Bogstad *et al.* [**34**] obtained steady-state airwake data for six different ships of the Royal Navy for a helicopter flight simulator by performing inviscid flow simulations. As commented by Zan [**35**], the incorporation of the time-accurate airwake is important for a high-fidelity flight simulation, and the changes in the wind direction need to be considered for a reasonable validation of CFD.

Guillot and Walker [**15**] solved the unsteady compressible Euler equations to investigate the unsteady airwake over LPD-17 and compared the results with the scaled-model wind tunnel measurements. In addition, the unsteady airwake and exhaust gas trajectories over highly complex ship superstructures were computed over DDG-51 Flt-IIA by Landsberg *et al.* [**36**] using FAST3D flow solver and over LPD-17 by Camelli *et al.* [**37**, **38**] using large eddy simulations (LES). Polsky and Bruner [**6**] and Polsky [**7**, **39**] performed steady and unsteady simulations of LHA ship airwakes using different numerical methods such as monotone integrated large eddy simulation (MILES) approach as well as k–ω and shear stress transport turbulence modelling. Polsky also studied the importance of the grid quality and atmospheric boundary layer modelling in reference [**39**] for the airwake simulations for beam (90°) winds. The atmospheric boundary layer was modelled as a far-stream inflow/outflow boundary condition while considering enough grid resolution over the ocean surface plane, and improved the comparisons of the predictions with the full-scale experimental data. Recently, Arunajatesan *et al.* [**40**, **41**] have conducted some preliminary steady/unsteady calculations of the LHA ship airwake using MILES approach.

In addition to the airwake computations, there have been several computational studies on ship airwake/helicopter rotor or fuselage flow interactions by Zan and Syms [**42**], Landsberg *et al.* [**43**], Tattersall *et al.* [**44**], and Wakefield *et al.* [**45**]. Arunajatesan *et al.* [**40**] calculated the flow field of the AV-8B outwash for various hover altitudes, and they are also planning to study the interaction of vertical/short takeoff and landing (V/STOL) and ship airwake flow fields.

Previously, at the Pennsylvania State University, Liu and Long [**46**], and Long *et al.* [**47**] used the non-linear disturbance equations approach (without viscous terms) to solve for the unsteady fluctuations over the generic SFS using both structured and unstructured grids. Modi [**48**] simulated the steady-state ship airwakes over SFS, CVN-75 and LHA classes of ships. Sharma and Long [**49**] have performed inviscid airwake simulations over LPD-17. Current inviscid, steady and unsteady CFD simulations of LPD-17 and LHA airwakes for different WOD conditions are discussed in detail in this article, whereas some preliminary results were presented in references [**1**–**3**, **49**, **50**].

1.2 Previous work on blade sailing

Blade sailing is one of the important problems of helicopter shipboard operations and is often observed when operating a helicopter from a ship deck. In severe conditions, blade sailing may result in catastrophic ‘tunnel strike’ (for tandem rotor configurations) or ‘tailboom strike’ (for single-rotor configurations) which can severely

damage the rotor blades and also cost lives. These problems occur before takeoff during rotor engagement and after landing during rotor disengagement. During these operations, the helicopter rotor is rotating at low speeds and so the centrifugal forces are small. The weak centrifugal force cannot offer enough resistance to the impulsive lift/drag force which can cause large-amplitude oscillations of the blades in longitudinal/lateral direction. The problem is aggravated when operating from a ship deck because of the flow separation from the sharp edges of the mast, the deck, and the hangar. The shedding of vortices from the edges characterizes the time variation of the flow over the deck. There is a chance that the shedding frequency will match the angular frequency of the rotor and excite the blades in resonance. This may amplify the deflections to such a level that it strikes the tailboom or fuselage. The vertical wind velocity through the rotor disc is the main contributor to the impulsive forces as it directly alters the angle of attack of the blades.

The problem of blade sailing has been addressed by many experimental [**51**–**55**] and analytical [**52**, **54**–**69**] investigations. Theoretical analyses tools for transient aeroelastic blade response during engage/disengage operations have been developed for different rotor systems: for teetering and articulated rotors with flap and droop stops by Newman [**59**], for articulated and hingeless rotor systems by Geyer and Smith [**61**, **62**], and for multi-bladed gimballed tiltrotors by Kang and Smith [**63**] and Smith *et al.* [**64**]. Newman [**59**], Keller and Smith [**65**], and Keller [**67**] attempted to model the velocity distribution over the deck using simple linear models. They concluded that such simplified models cannot accurately predict the severe blade sailing observed in practice. This presents the need to obtain the 'real' airwake data either experimentally or numerically.

1.3 Previous DI studies

Ship/helicopter DI simulations have been studied [**1**–**5**, **21**, **34**, **70**–**83**] to investigate the pilot workload and response during the shipboard operations, to develop safe WOD flight envelopes and flight trajectories for any ship/helicopter combination, and to develop helicopter flight simulators for pilot training and engineering purposes. In DI simulations, the modelling problems include helicopter flight dynamics, rotor aerodynamics and fuselage loads, flight control systems, ship motion, ship airwake flow (usually as gust penetration models), and a human pilot workload and response model.

As addressed by Healey [**70**], the simulation of the airwake is the most challenging and computationally intensive task in numerically simulating the ship/helicopter DI. Healey also highlighted the need for more accurate experimental data on real ships. Recent studies on flight dynamics simulations have used experimental data [**21**] and/or the numerical data, e.g. the steady-state airwake [**34**, **77**] and the unsteady airwake [**1**–**3**, **76**, **80**] data from CFD simulations. A stochastic representation of the unsteady airwake may be another alternative [**77**, **80**]. As stated by Zan [**35**], the incorporation of the time-accurate airwake is important for a high-fidelity flight simulation. Lee *et al.* [**3**] performed LHA ship airwake and DI simulations for UH-60A landing, takeoff, and station-keeping, and showed that the time-varying airwake has significant effect on pilot control activities during shipboard operations.

McKillip *et al.* [**82**] described a DI simulation tool in which a real-time, free-wake rotor flow field is coupled with panel-based fuselage and ship flow fields, thus considering the interactional aerodynamics of V-22 tiltrotor operating over an LHA class ship. He *et al.* [**83**] performed a similar study for shipboard landing simulation of CH-46 rotorcraft.

2 SHIP AIRWAKE CFD SIMULATIONS

Computational fluid dynamics (CFD) is used in this article to simulate the airwakes of two different classes of ships: LHA and LPD-17. Parallel, time-accurate CFD simulations have been performed for several WOD conditions: a relative wind speed of 15.43 m/s (30 knot) and WOD angles of 0°, 30°, 45°, 90°, 270°, and 315°.

The LHA/LHD class US Navy ships, which resemble small aircraft carriers, are the largest of all amphibious warfare ships. The LHA/LHD ships are

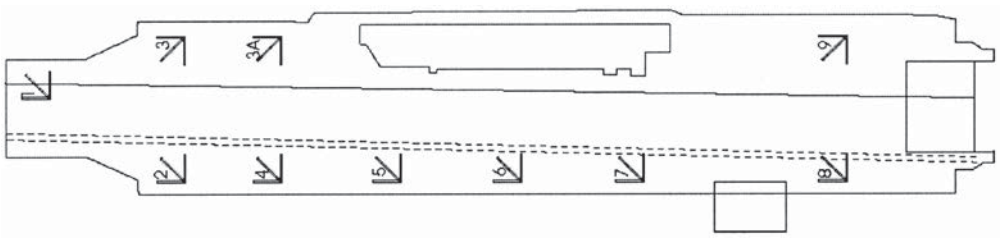

Fig. 1 Top view of an LHA class ship showing the landing spots on the ship deck [**3**]

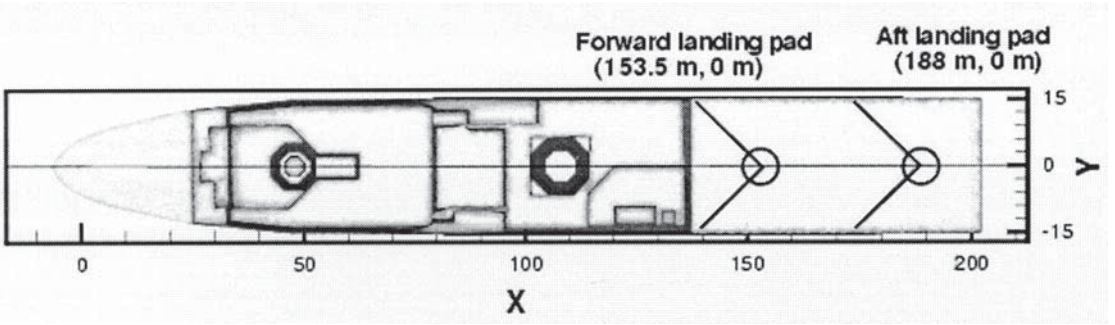

Fig. 2 A sketch showing the position of the two landing pads on the LPD-17 ship

capable of shipboard operations of V/STOL, short take off vertical landing type aircraft such as AV-8B Harrier and F-35 joint strike fighter, and vertical takeoff and landing tiltrotor and rotary wing aircraft such as the MV22-Osprey tiltrotor, UH-1 Huey, AH-1 Super Cobra, CH-46 Sea Knight, and CH-53 Sea Stallion helicopters. A few details of the Tarawa LHA class ship are provided in the Appendix.

Figure 1 shows the top view of an LHA class ship and the landing spots on the ship deck. The main features of the ship are the ship's superstructure on the starboard side and the elevator on the port side. There are ten landing spots on the deck as shown in the figure. The landing spot 8 that is just behind the elevator was investigated in references [**1**–**3**] as a target spot for shipboard operations. Landing spots 2 and 7 are considered in this article.

The San Antonio LPD-17 is the US Navy's newest class of ship. It is a warfare capable ship but its primary mission is the amphibious transport of marines and cargo. The prominent features which mark the geometry of LPD-17 are the two masts one behind the other separated by a distance of $\sim$90 m. There are two landing spots on the deck for the shipboard operations of helicopters and V/STOL aircraft. Figure 2 shows the two landing spots on the deck of the LPD-17 ship. The front landing pad is located on the centre-line at $X = 153.5$ m (the origin is at the point where the bow intersects the waterline), and the aft landing pad is at $X = 188$ m. A few details on this ship are provided in the Appendix.

The unstructured three-dimensional finite-volume flow solver used for the CFD simulations performed in this article, the details of the unstructured grids generated for the full-scale ship models, and the boundary conditions applied and the parallel computers used for the simulations are discussed subsequently.

2.1 Flow solver: PUMA2

PUMA2 is a modified version of the flow solver PUMA (parallel unstructured maritime aerodynamics CFD solver) [**84**] which uses a finite-volume formulation of the Navier–Stokes equations for three-dimensional, internal and external, non-reacting, compressible, unsteady, or steady-state solutions of problems for complex geometries.

The Navier–Stokes equations may be written in an integral form for a space volume V bounded by a surface S as

$$\frac{\partial}{\partial t}\int_V Q\,\mathrm{d}V + \int_S (\boldsymbol{F}\cdot\boldsymbol{n})\,\mathrm{d}S - \int_S (\boldsymbol{F}_\mathrm{v}\cdot\boldsymbol{n})\,\mathrm{d}S = 0 \tag{1}$$

$$Q = \begin{Bmatrix} \rho \\ \rho u_1 \\ \rho u_2 \\ \rho u_3 \\ \rho e_0 \end{Bmatrix}, \quad F_j = \begin{Bmatrix} \rho u_j \\ \rho u_1 u_j + p\delta_{1j} \\ \rho u_2 u_j + p\delta_{2j} \\ \rho u_3 u_j + p\delta_{3j} \\ \rho h_0 u_j \end{Bmatrix},$$

$$F_{\mathrm{v}j} = \begin{Bmatrix} 0 \\ \tau_{1j} \\ \tau_{2j} \\ \tau_{3j} \\ (u_1\tau_{1j} + u_2\tau_{2j} + u_3\tau_{3j}) - q_j \end{Bmatrix} \quad j = 1, 2, 3$$

where $\boldsymbol{Q}$ is a column vector of the flow variables in a conservative form, $\boldsymbol{F}$ the inviscid flux vector, and $\boldsymbol{F}_\mathrm{v}$ the viscous flux vector. τ_{ij} is the viscous stress tensor, and q_j is the heat flux. Pressure, total energy, and total enthalpy are given by

$$p = (\gamma - 1)\rho e, \quad e_0 = e + \frac{1}{2}\boldsymbol{u}\cdot\boldsymbol{u}, \quad h_0 = e_0 + \frac{p}{\rho} \tag{2}$$

Mixed topology unstructured grids composed of tetrahedra, wedges, pyramids, and hexahedra are supported in PUMA2. Different time integration and iterative algorithms such as Runge–Kutta, Jacobi, and various Successive over-relaxation schemes (SOR) are also implemented. It is written in ANSI C/C++ using the message passing interface (MPI) library to run in parallel. PUMA2 can be run so as to preserve time accuracy or as a pseudo-unsteady formulation to enhance convergence to steady state.

PUMA2 is also compatible with C++ compilers and coupled with the computational steering and monitoring library, portable object-oriented scientific steering environment (POSSE) [**85**, **86**]. PUMA2 solves the steady/unsteady Euler/Navier–Stokes equations on unstructured stationary or moving grids (i.e. rotation about an axis) [**85**]. LES with or without wall models can also be performed with PUMA2 [**87**, **88**]. PUMA2 has been used for all results presented in this article.

2.2 Unstructured grids

For complicated geometries, such as the LHA and the LPD-17 ships, unstructured grids are preferred because the unstructured grids can resolve the complex bodies better without excessive grid size and the grids are relatively easy to generate when compared with structured grids. The grids used for the simulations of both ships were generated using Gridgen [**89**]. The computations are performed for full-scale ships. Beacuse the time step for time-accurate computations (using an explicit scheme) is determined by the smallest cell in the volume grid, a fairly uniform surface grid was chosen on both ships. Hence, the minimum cell size and maximum number of cells were selected during the grid generation process by also considering the total computational time needed for the time-accurate simulations. Although a systematic grid dependence study is not reported here, the grid size considered here was found to resolve the flow features accurately. In addition, this flow solver has been carefully validated on several different applications using unstructured grids [**86**–**88**].

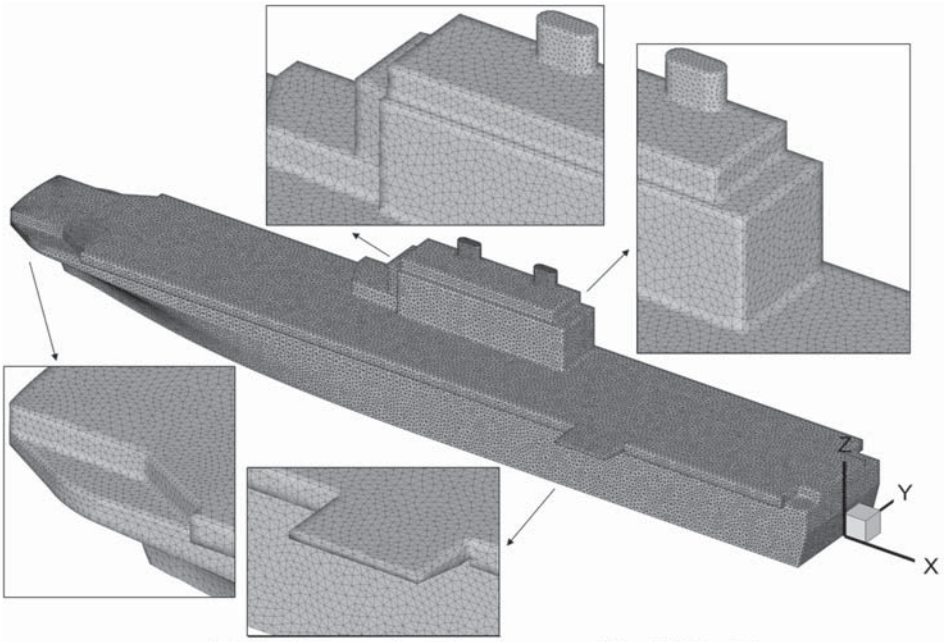

(a) Surface mesh and geometry of the LHA ship

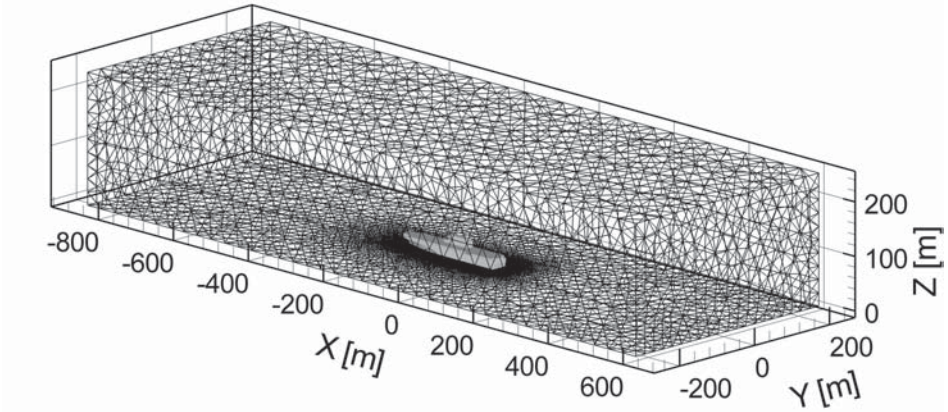

(b) Computational domain

Fig. 3 The computational grid used for the LHA ship airwake simulations

The full-scale LHA geometry model used in the simulations is 250 m ($L = 820$ ft) in length. The ship is approximately 36 m wide (W), extending from -18 to $+18$ m in y. The flight deck height (H) is $\sim$20 m. Figure 3(a) shows the surface mesh of the LHA which is composed of almost uniform-size triangles. The rectangular computational domain, which is shown in Fig. 3(b), has approximately 850 K tetrahedral cells with clustering around the ship. The bottom surface of the domain is the waterline ($Z = 0$). The computational domain extends approximately $2.4 \cdot L$ both in front and behind the ship. The side outer boundaries are $6.8 \cdot W$ away from the centre-plane ($Y = 0$). The upper outer boundary is $12.4 \cdot H$ away from the waterline. The minimum cell length is $\sim$0.04 m which gives a time step of 0.48 ms for a Courant–Friedrichs–Lewy (CFL) number of 0.8 (using Mach number scaling).

Figure 4(a) shows the surface mesh on the LPD-17. Clustering is done all around the ship with increasing cell size towards the boundaries of the bounding box. The computational domain extends to a distance of $2 \cdot L$ both in front and behind the ship, where $L = 200$ m is the ship length. The side outer boundaries are at a distance of $7 \cdot$ W from the centre-plane, where $W = 30$ m is the width of the ship deck. The waterline is taken to be the bottom surface of the bounding box. The upper outer boundary is at a distance of $6 \cdot H$ from the waterline, where $H = 50$ m is the maximum height of the ship. Figure 4(b) shows the size of the bounding box in relation to the size of the ship, and also the surface grid on the outer boundaries. The total number of tetrahedra in the volume grid is around 760 K. The minimum cell length is about 0.1 m which gives a time step of 1.22 ms for a CFL number of 0.8 (using Mach number scaling).

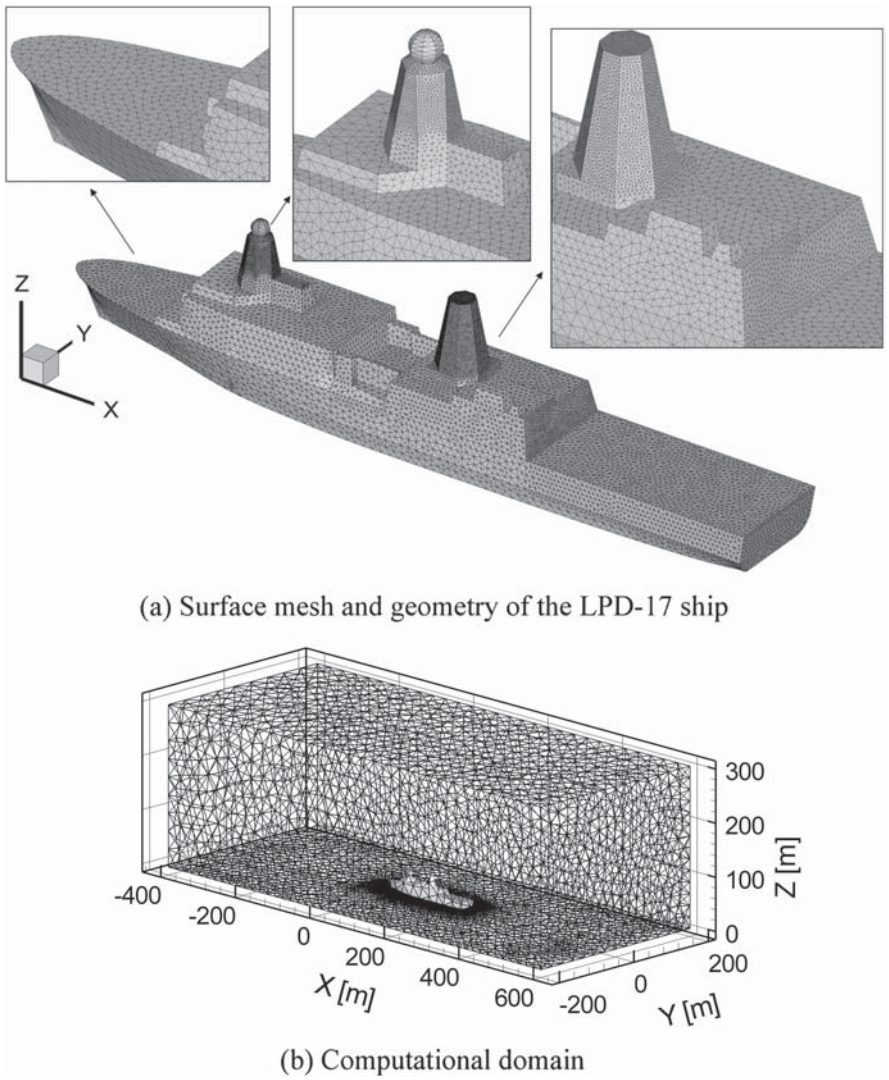

Fig. 4 The computational grid used for the LPD-17 ship airwake simulations

2.3 Boundary conditions

Because the flow is assumed to be inviscid, a zero-normal velocity condition is imposed on the ship surface. The waterline which is the bottom face of the bounding box (for both ships) is also assigned the zero-normal velocity condition. A Riemann boundary condition is used on the other five faces of the bounding box to avoid any reflections into the domain.

2.4 Parallel computers

All the simulations for this article were performed in parallel on the following Beowulf clusters at

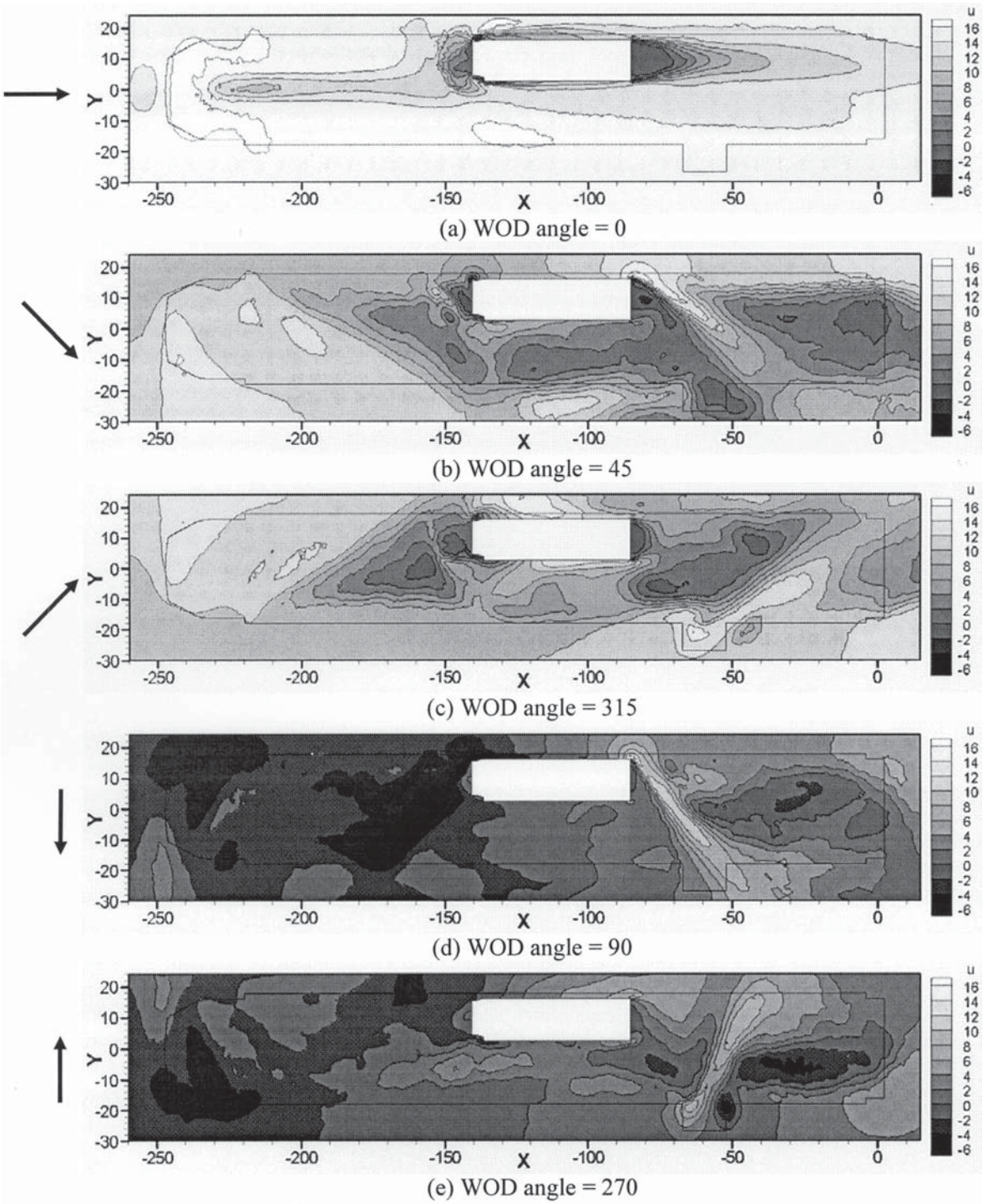

Fig. 5 Contours of the *X*-component of velocity (m/s) in a plane 6 m above the LHA deck for different WOD angles. The solid lines represent the boundary of the ship geometry below. The arrows indicate the direction of incident flow

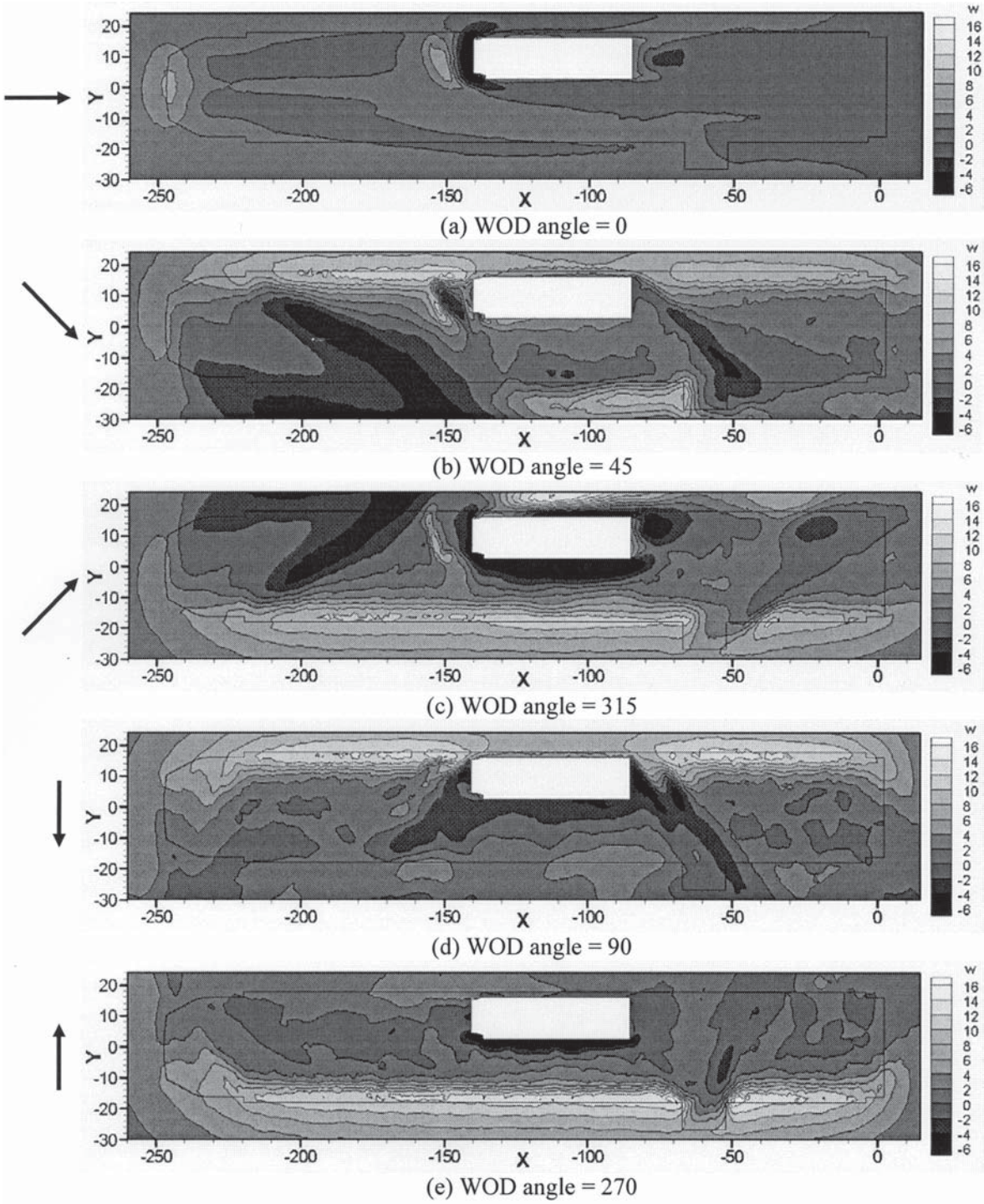

Fig. 6 Contours of the *Z*-component of velocity (m/s) in a plane 6 m above the LHA deck for different WOD angles. The solid lines represent the boundary of the ship geometry below

The Pennsylvania State University: cost effective computing array-3 (COCOA3), LION-XL, and MUFASA. COCOA3 is a parallel PC cluster consisting of 60 nodes with dual 2 GHz Intel Xeon processors. Each node has 2 GB of random access memory (RAM) and the nodes are interconnected by a Gigabit Ethernet network. LION-XL has 128 compute nodes with dual 2.4 GHz Intel P4 processors, 4 GB ECC RAM and Quadrics high-speed interconnect. MUFASA has 85 computational nodes with dual MP2200+ MHz Athlon processors and 1 GB RAM. The nodes are connected both by an Ethernet and by a high-speed Scali Dolphin network.

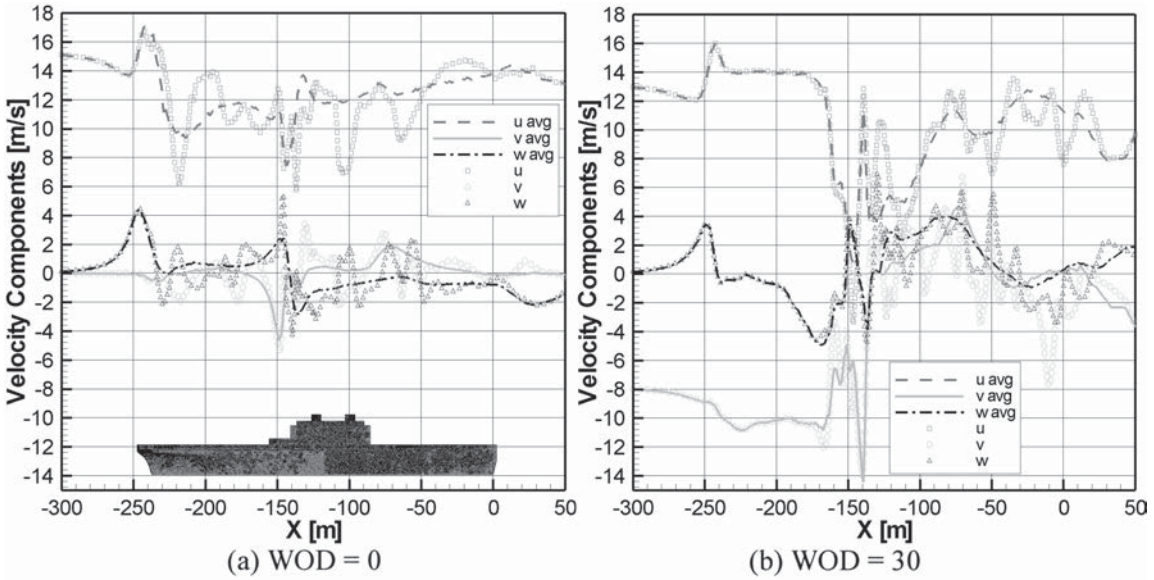

Fig. 7 Distributions of the time-average and the instantaneous velocity components along the centre-line, 6 m above the LHA ship deck for 0° and 30° WOD angles

3 RESULTS

3.1 LHA airwake simulations

The steady and unsteady airwake predictions for the full-scale LHA class ship were obtained for a relative wind speed of 15.43 m/s (30 knot) and several WOD angles. A four-stage Runge–Kutta explicit time integration algorithm with Roe's flux-difference scheme was used with CFL numbers of 2.5 and 0.8 for the steady and unsteady computations, respectively. The pseudo-steady-state computations were performed using local time stepping and initialized with the freestream conditions. The time-accurate computations were started from the pseudo-steady-state solution. It required nearly 2000 iterations to simulate 1 s of real flow (which took ∼1.8 h on 12 processors of LION-XL).

The time-accurate inviscid simulations for 0°, 45°, 90°, 270°, and 315° WOD cases were performed on COCOA3 and LION-XL. The simulations were performed for a total of 18 real-time seconds. The flow properties were sampled every 0.1 s, and then time-averaged to obtain a 'steady-state' solution. Figures 5 and 6 present the contour plots of the time-averaged velocity data for different WOD angles to show the range of velocity scales of the ship airwake above the deck. Figure 5 shows the contours of 'X'-component of velocity (the axial velocity component), on an X–Y plane 6 m (20 ft) above the deck. The solid lines represent the boundary of the ship below. This plane intersects the superstructure of the ship, hence, that area is left empty in Figs 5 and 6. This should not be confused with the white colour representing the highest contour value in the plots. The front part of the ship, ahead of the superstructure is symmetric about the centreline. The geometric symmetry results in symmetric flow patterns as seen in Figs 5(b) and (c). However, the flow is very different around the superstructure and in the aft of the ship (with respect to the incident wind) for WOD = 45° and 315° because of the asymmetric location of the superstructure. For WOD = 45°, landing spot 7 is directly in the wake of the superstructure, whereas for WOD = 315°, it is upstream of the structure and experiences a more steady wind.

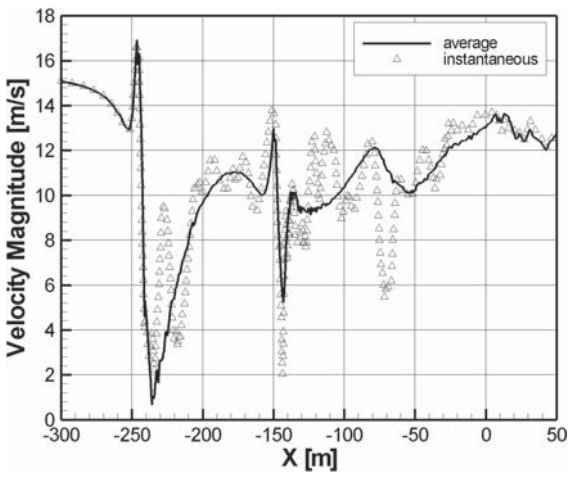

Fig. 8 Distributions of the time-average and the instantaneous velocity magnitude, $(u^2 + v^2 + w^2)^{1/2}$ along the centre-line, 3 m above the LHA ship deck for 0° WOD angle

Contours of the 'Z'-component of velocity (the vertical velocity component) are shown in Fig. 6. The Z-component of velocity is important because it directly affects the angle of attack (and hence the lift) of a blade. The different landing spots experience a wide range of 'Z' velocity for different WOD angles. The spots on the port side of the ship experience very high positive Z velocities for WOD = 315° and 270°, and those on the starboard side for WOD = 45° and 90°. A pilot has to take this into account when trying to land/takeoff a helicopter from these landing pads. In addition, because a rotor diameter is very big, the spatial variation of Z velocity (and hence the lift) may result in an unbalanced loading of the rotor and an extra

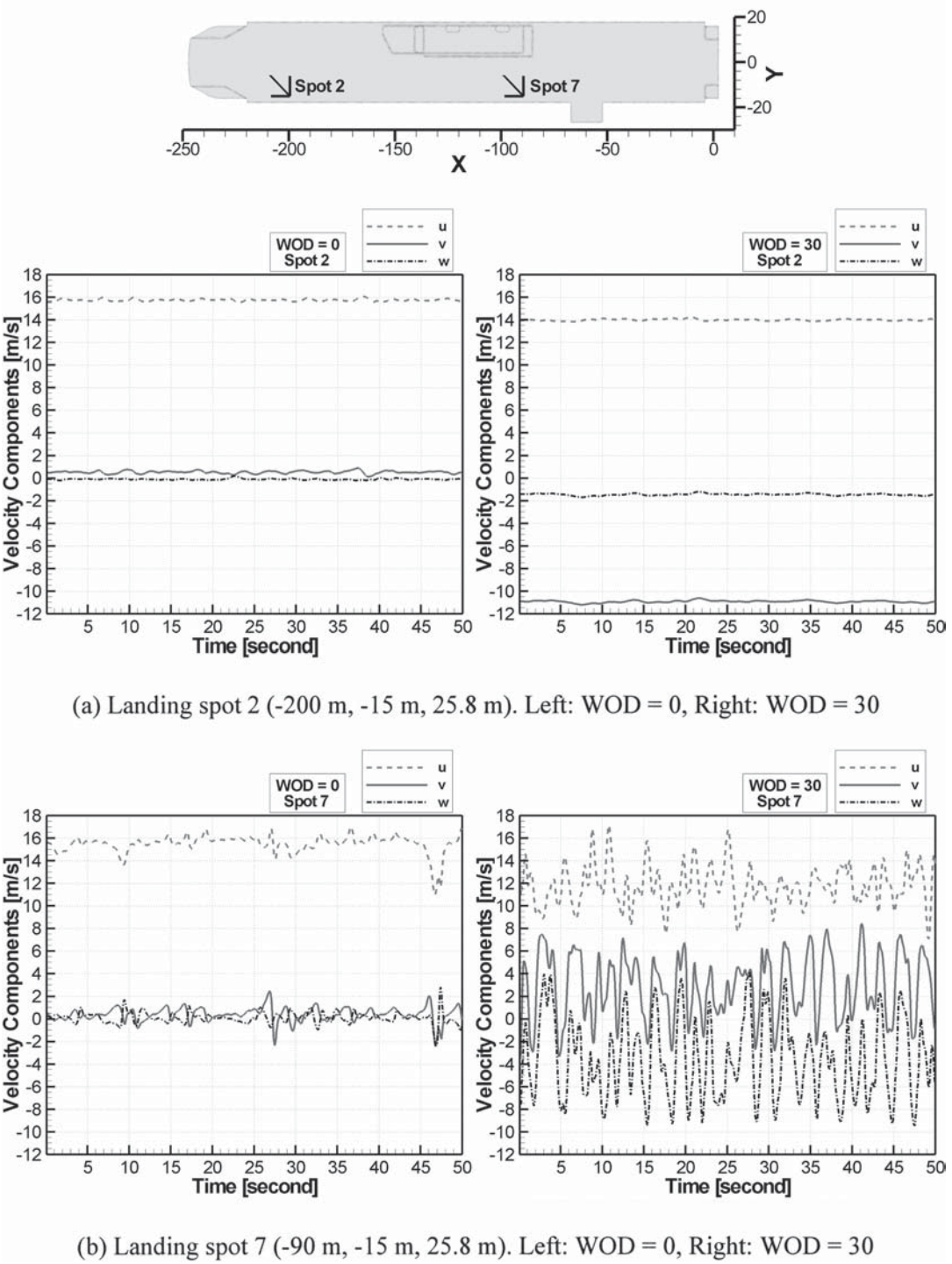

Fig. 9 Time history of the velocity components in the X, Y, and Z-directions, 6 m above the landing spots 2 and 7 of the LHA for two WOD angles

workload for the pilot to compensate for it. Adding to this, the gusty winds and the rolling deck motion make the task more intimidating and hazardous.

Time-accurate flow simulations were also performed for 0° and 30° WOD cases for a total of 50 s of real flow in a relative wind of 15.43 m/s (30 knot). Figure 7 shows the velocity components along the centre-line, 6 m above the deck of the LHA ship for 0° and 30° WOD angles. The lines represent the time-averaged solution and the symbols represent an instantaneous solution. The time average is calculated over a period of 50 s. A comparison of the time-averaged data against the data at an instant illustrates the level of fluctuations in the flow field. The large spatial variation in the velocity, especially the high gradients around $X = 150$ m, may result in unsteady loading on a Harrier or V-22 operating from the ship.

Figure 8 shows the distributions of the averaged and instantaneous velocity magnitude along the centre-line 3 m (10 ft) above the ship deck. The distribution of the velocity magnitude for the 0° case is similar to the CFD results in reference [**7**] which were compared to the experiments.

The time histories of velocity components, (u, v, w), 6 m above the two landing spots (that is at $z = 25.8$ m) for the two WOD angles are shown in Fig. 9. The landing spot 2 $(-200, -15, 25.8$ m) is located in front of the deck, and the spot 7 $(-90, -15, 25.8$ m) is located in the wake of the superstructure of the LHA ship (for WOD = 30°). At spot 2 (Fig. 9(a)), the magnitudes of the velocity components differ with wind direction and speed. For WOD = 30°, it is observed that the magnitude of the 'Y'-component of velocity at spot 2 (i.e. −11 m/s) is ∼40 per cent higher compared with the Y-component of the freestream (i.e. −7.7 m/s). This is most probably due to the coherent oblique

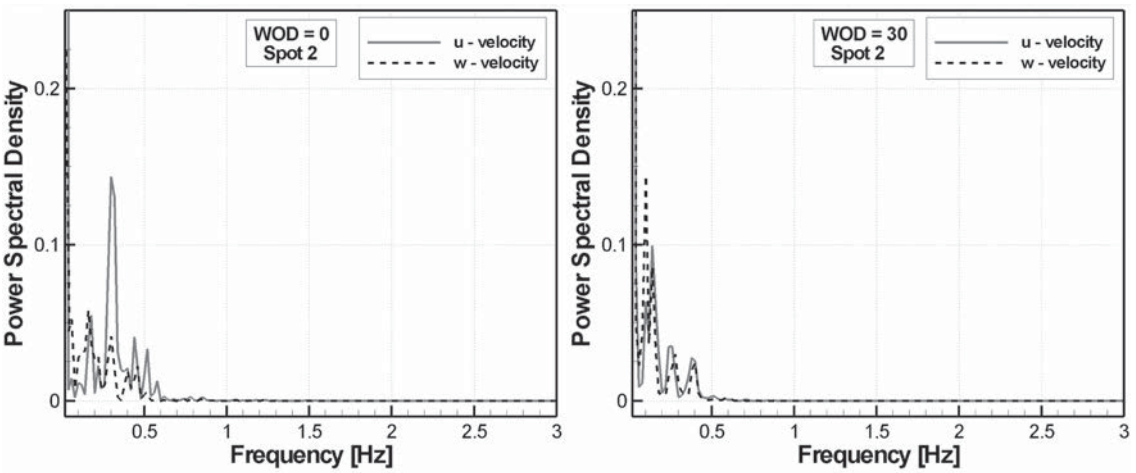

(a) Landing spot 2 (–200 m, –15 m, 25.8 m). Left: WOD = 0, Right WOD = 30

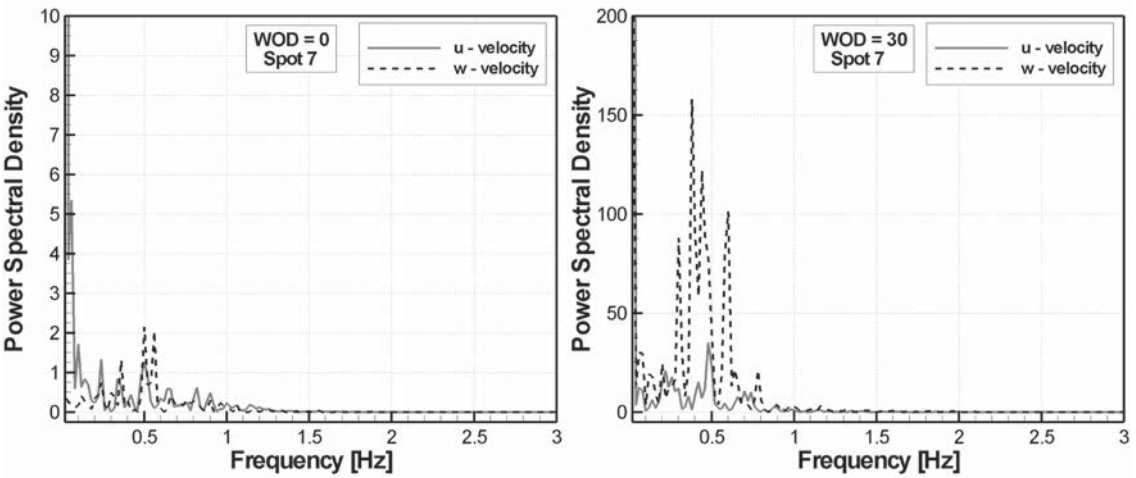

(b) Landing spot 7 (–90 m, –15 m, 25.8 m). Left: WOD = 0, Right WOD = 30

Fig. 10 PSDs of the velocity components in the X and Z-directions 6 m above the two landing spots of the LHA ship for two WOD angles

vortical structure over this spot, as observed from the vorticity iso-surfaces that will be presented later in this article. There is also elevated negative vertical velocity ($\sim$1.5 m/s towards the deck) for the 30° case, whereas for 0° case, the vertical velocity is positive and $<$1.0 m/s. These variations in flow field with WOD conditions may influence the loads on the helicopter rotor as well as the fuselage.

Although velocity levels change with WOD conditions over spot 2, the flow is almost steady and the fluctuations are minimal. In contrast, the fluctuations are much larger for spot 7, especially for WOD = 30° case (Fig. 9(b)). Variations in magnitude as large as 8 m/s for *X*-component of velocity and as large as 13 m/s for '*Z*'-component of velocity can be observed. These results clearly show the unsteadiness of the flow field over spot 7, which may significantly affect the flight dynamics of rotorcraft operating over this region as well as the pilot workload.

The power spectral densities (PSDs) (square of the magnitude of the Fourier transform of velocity data) of the *X* and *Z*-components of velocity are plotted in Fig. 10. Because the fluctuations at the two landing spots differ greatly, the scales used in plotting the PSDs for the two landing spots are different. A few discrete peaks can be observed in the spectra in the frequency range 0–1. For landing spot 2, the peak frequencies are observed around 0.1 and 0.3 Hz, and for landing spot 7, the peak frequency is $\sim$0.5 Hz. This is in general agreement with the results of Polsky [**7**] where the observed frequencies are in the same range. The strong airwake velocity fluctuations about once every 2 s (0.5 Hz) may present a strong challenge to the pilot in control activities. As the peaks in the spectra occur at very low frequencies ($<$1 Hz), longer time records may be required to better resolve the spectra. In addition, pilot workload is associated with low frequency, so it is important to compute

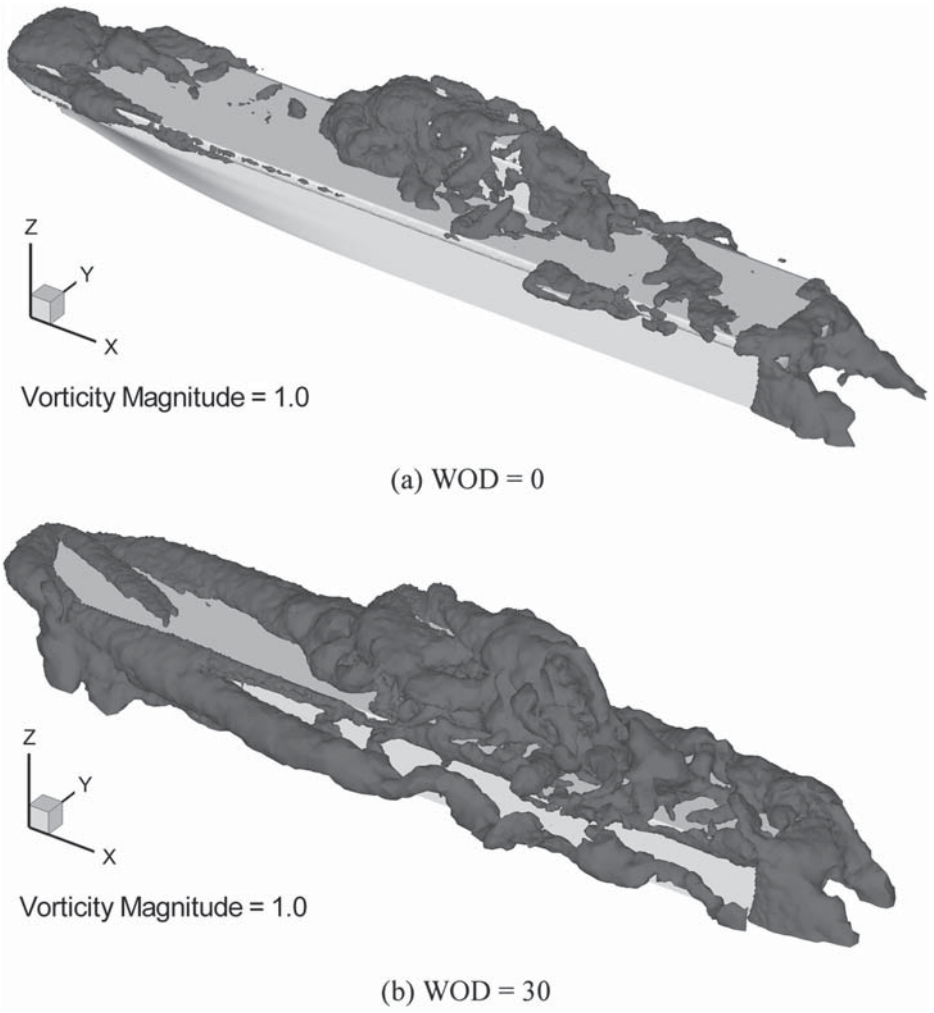

Fig. 11 Instantaneous iso-surfaces of vorticity magnitude of 1.0 s^{-1} around the LHA for 0° and 30° WOD angles

longer simulations in the future. It is also possible that PSDs computed from a sufficiently long-time record would show much smoother spectra. Wind tunnel experiments can generate long-time histories, and those results should be used together with CFD to develop a complete understanding of ship airwake flow fields.

Figure 11 shows the instantaneous iso-surface of vorticity magnitude of $1.0\,s^{-1}$ around the LHA for 0° and 30° WOD angles. The iso-surfaces show the turbulent eddies that are continuously formed around the sharp edges of the ship boundaries and the superstructure. These eddies convect downstream with the wind and are responsible for the unsteady fluctuations observed in the downstream region. These unsteady flow features can be better observed by creating an animation of iso-surfaces in time, and stereographics displays can be useful to visualize and better understand the details of such complex flows [**86**, **90**]. The complex flow features of the airwake can be identified as deck-edge vortices, bow separation, separated vortical regions on the deck (e.g. burbles between the bow separation and the island for the 0° case), and

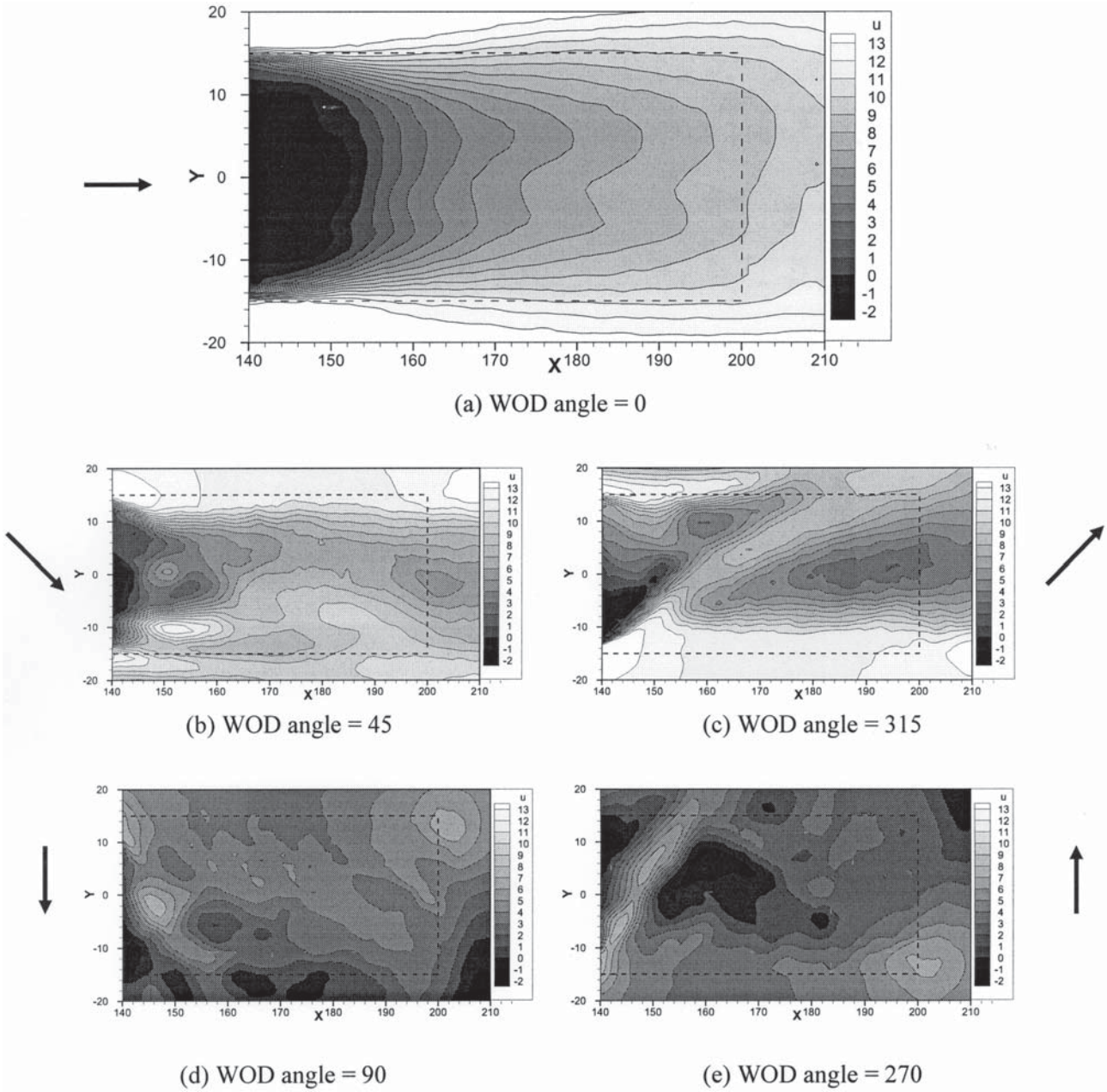

Fig. 12 Contours of X-component of velocity (m/s) in a plane 5 m above the LPD-17 deck for different WOD angles. The dashed line represents the boundary of the ship deck below

complex island wake. For the case of WOD = 30°, much more complicated eddy structures can be observed, especially over landing spots 7 and 8 in the island wake. Furthermore, an oblique coherent vortical structure, which is shed from the bow and starboard side edge intersection, is clearly evident over landing spot 2.

3.1.1 *DI Simulations*

The time-accurate CFD data from the LHA ship airwake simulations for 0° and 30° WOD cases were also used for a target spot of shipboard operations as described in references [**1**–**3**]. In these LHA ship/UH-60A helicopter DI simulations, the landing spot 8 was investigated as the target spot for the specified departure and approach operations. The pilot control activity was simulated using an optimal control model of the human pilot. Only the last 40 s of the time-accurate CFD data was used for the DI simulations. The velocity field data for a smaller DI domain over the selected landing spot was extracted by post-processing the stored flow data. Each CFD flow solution file was 41 MB in size, whereas the velocity data (a total of 400 instants of time with 0.1 s of interval) required in the DI simulations was only 5.2 MB for

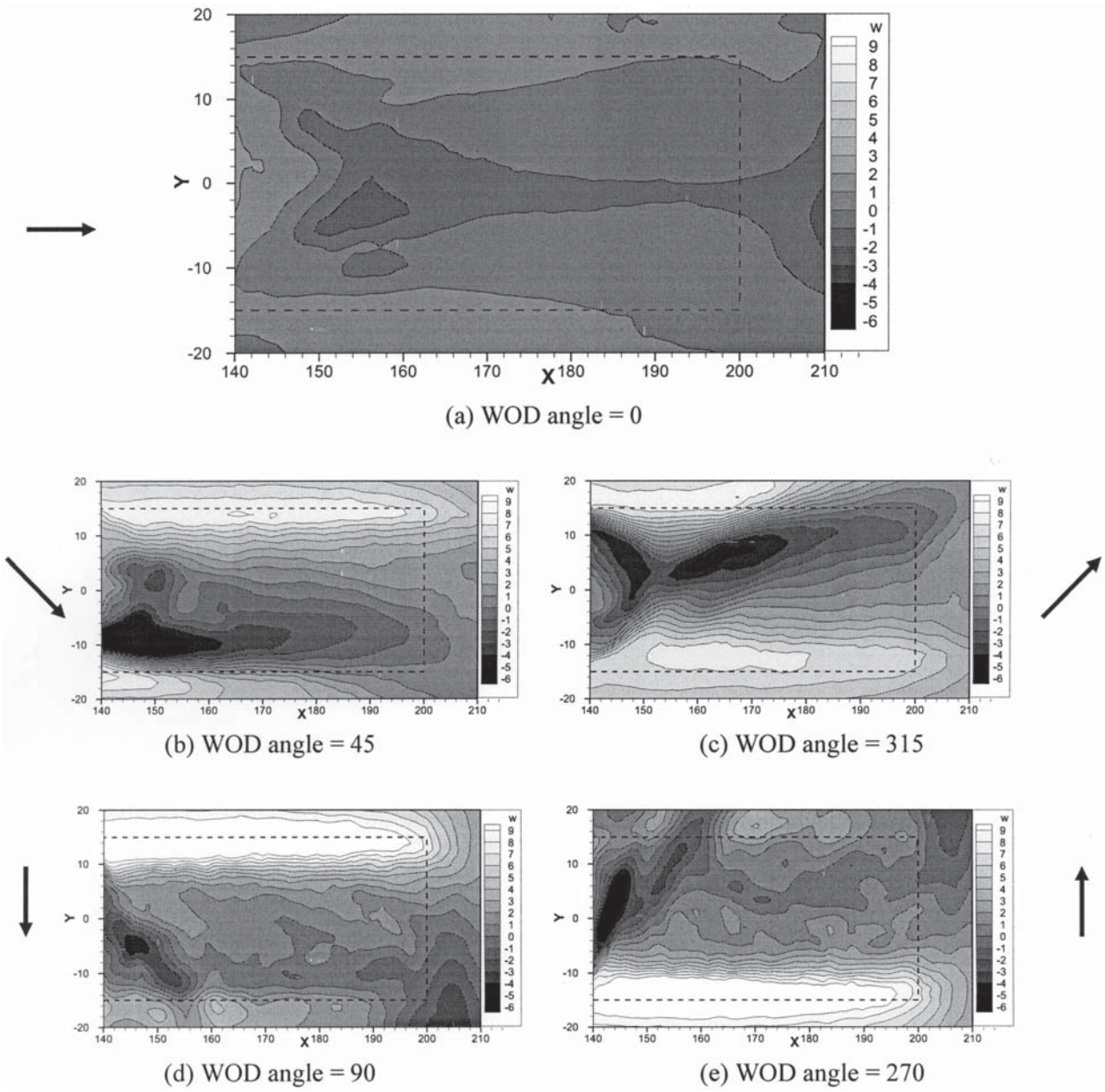

Fig. 13 Contours of *Z*-component of velocity (m/s) in a plane 5 m above the LPD-17 deck for different WOD angles. The dashed line represents the boundary of the ship deck below

each instant. The time-varying velocity field data were used in the gust penetration model to find the disturbances at various locations on the helicopter as varying both spatially and temporarily in the DI simulations. Thus, the rotor inflow, fuselage forces were affected by the ship airwake; however, the ship airwake was not affected by the rotor and fuselage wakes.

The results of the DI simulations clearly indicated that the time-varying ship airwake has a significant impact on aircraft response and pilot control activity when the helicopter is operating in or near a hover relative to the ship deck (station-keeping) over the selected spot. In addition, the results for the 30° WOD case showed significantly larger oscillations in the aircraft attitude responses and pilot control inputs than for the 0° case. Lee *et al.* [**3**] also discussed the difficulties in handling the large quantities of airwake data.

3.2 LPD-17 airwake simulations

The flow over the San Antonio class LPD-17 ship was also simulated using the flow solver PUMA2. The inviscid computations were performed on PC clusters COCOA3 and MUFASA. The time-accurate solutions were obtained by using the four-stage Runge–Kutta algorithm with Roe's scheme with a CFL number of 0.8.

To investigate the effect of wind direction, time accurate runs were performed for five different WOD angles: 0°, 45°, 315°, 90°, and 270°. As the flow is highly unsteady, the solution does not converge to a single steady state. To correctly represent the behaviour, a time average over 14 s of data, which were stored every 0.1 s, is obtained. At a speed of 15.43 m/s (30 knot), the flow sweeps through a ship-length (200 m) in <14 s. Hence, it is expected that a period of 14 s is sufficient to capture the unsteadiness in the flow. Figure 12 plots the contours of velocity in X-direction on a plane 5 m above the deck of the ship for different WOD angles. The dashed lines represent the boundary of the ship deck below this plane.

The case of WOD = 0 is obtained by averaging over 40 s of data; all the other cases are time averages over 14 s of time accurate data. The wake in Fig. 12(a) is slightly asymmetric. This is because of the superstructure on the starboard side of the ship immediately before the hangar. A comparison of Figs 12(b) and (c) also reflects the asymmetry in the ship geometry about the centre-line. A similar comparison is made for the Z-component of velocity on the same plane in Fig. 13. The asymmetry in the ship is again reflected in Figs 13(b) and (c). For the WOD = 90 and 270 cases, a large variation in the velocity (Z-component) is observed as the flow climbs up (positive Z-velocity) near the side facing the flow and then bends down (negative Z-velocity) after crossing the deck. Figures 12 and 13 give a broad picture of the flow structure above the deck of the LPD-17 ship for different WOD angles.

Figure 14 provides a measure of unsteadiness in the flow over the deck. The time-averaged values of velocity components are compared with instantaneous

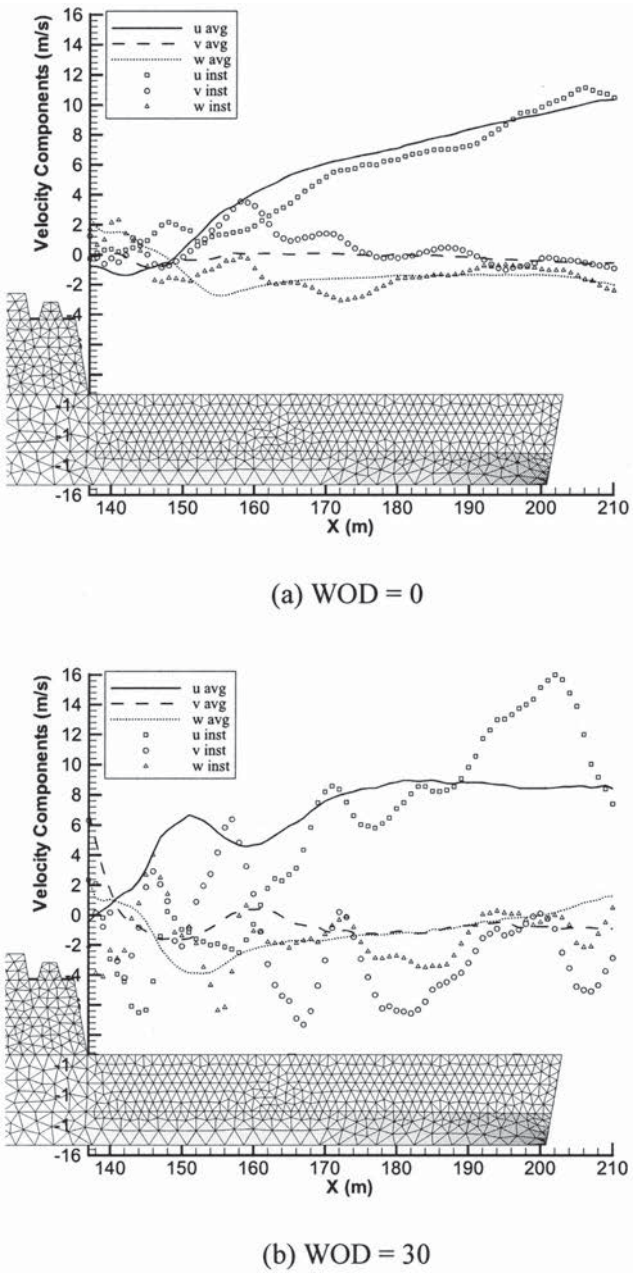

Fig. 14 Time-averaged and instantaneous velocity components on the centre-line 5 m above the deck of a LPD-17 ship for two WOD angles. The lines represent time-averaged solution and the symbols represent solution at an instant of time. The time average is calculated over a period of 40 s

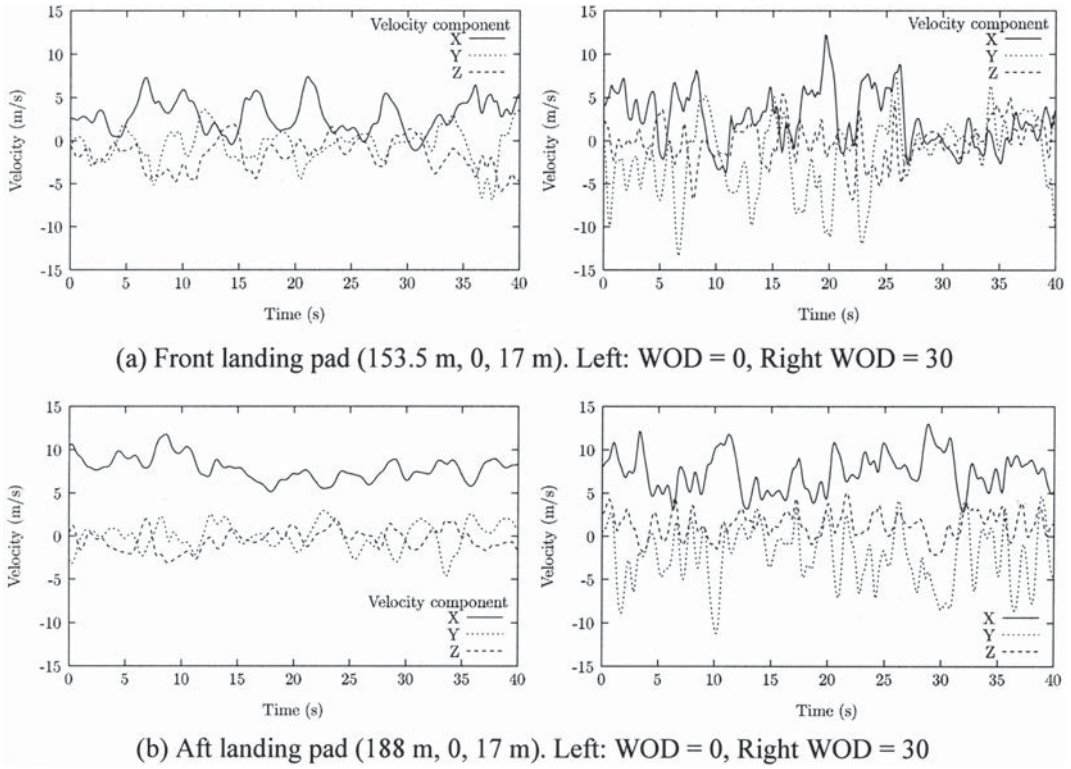

Fig. 15 Time history of the velocity components in the *X, Y,* and *Z* -directions 5 m above the front and aft landing spots of LPD-17 for two WOD angles

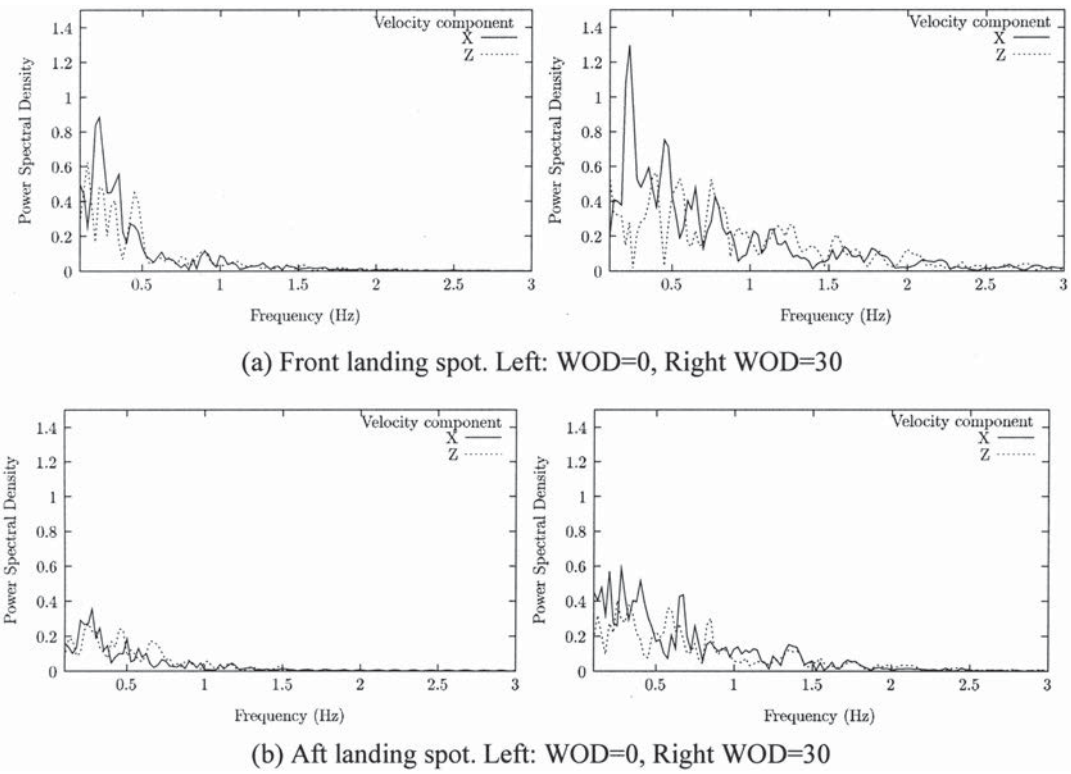

Fig. 16 PSD of the velocity components in the *X* and *Z*-directions at points 5 m above the two landing spots of the LPD-17 ship for two WOD angles

values. The instantaneous values deviate from the time-averaged solution significantly for both WOD cases. The overall fluctuations are found to be larger for the 30 WOD case in comparison to the 0 WOD case. This could be because for the 30 WOD case, the free shear layer (or even vortical structures) separates not only from the top and side of the hanger, but also from the edge of the deck (starboard side) as the flow approaches the ship at an angle.

Time histories of velocity components are plotted for two WOD angles at two points above the landing spots on the LPD-17 ship in Fig. 15. The points are taken to be 5 m above the ship deck. Figure 15(a) plots the histories for WOD = 0 and 30 above the front landing spot and Fig. 15(b) plots them above the aft landing spot. Velocity fluctuations as large as 7 m/s in the case of WOD = 0 and as large as 15 m/s for the WOD = 30 case are observed. Such large fluctuations in velocities can result in large fluctuations in blade loading and in blade sailing. The fluctuations are observed to be larger on the front landing spot than on the aft landing spot. This is expected because the front landing spot is nearer to the hangar and the ship rear mast; vortices shed from these structures are responsible for the observed velocity fluctuations.

To identify possible preferred frequencies of vortex shedding, Fourier transforms of the time accurate data (velocity components) were performed at the two landing spots (same as those in Fig. 15). The transforms were performed over data collected for 40 s of real flow. A Hamming window was used to filter out spurious frequencies. The PSDs for the two WOD cases are plotted for both front and aft landing spots. Multiple peaks can be observed in the spectra of the *X*-component of velocity (refer Fig. 16(a)) for frequencies <1 Hz, but the peak at 0.2 Hz is prominent on the front landing spot for both 0 and 30

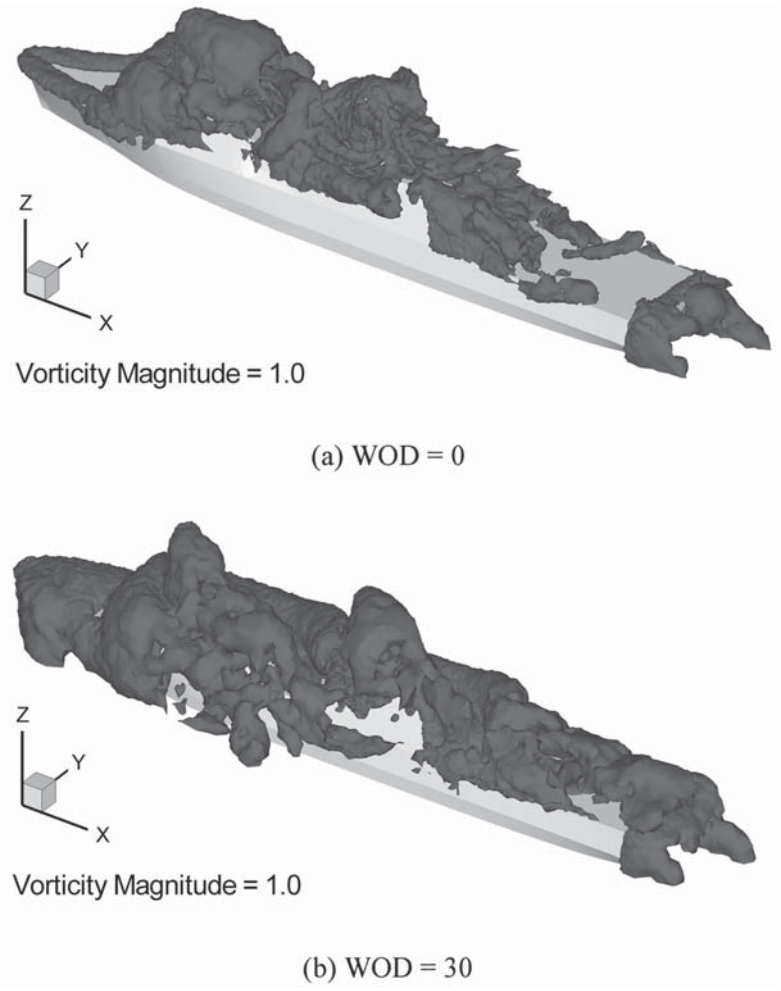

Fig. 17 Instantaneous iso-surface of vorticity magnitude of 1.0 s^{-1} around the LPD-17 for 0° and 30° WOD angles

WOD cases. Another peak at 0.5 Hz is observed in Fig. 16(a) for the 30 WOD case at the front landing spot. This peak could be related to the vortex shedding frequency from the edge of the hangar on the starboard side, whereas the peak at 0.2 Hz could be due to vortex shedding frequency of the aft mast of the ship. For the Z component of velocity, the spectra (Fig. 16(b)) have multiple peaks of comparable strength for both WOD cases at both landing spots.

Figure 17 shows the instantaneous iso-surface of vorticity magnitude of $1.0\,s^{-1}$ around the LPD-17 for 0° and 30° WOD angles. For WOD = 0 case (Fig. 17(a)), two coherent deck edge vortices at the bow section are clearly visible. It can be observed that the separated vortical structures shed from the front mast impact on the rear mast. This interaction may be the reason for the observed finer eddies in the wake of the rear mast and over the flight deck. For the WOD = 30 case, the wakes of the front and rear mast get convected separately with minimal interaction as seen in Fig. 17(b). For this case, the flow field over the flight deck is mostly dominated by the separated vortical structures shed from the starboard side of the deck and the hangar.

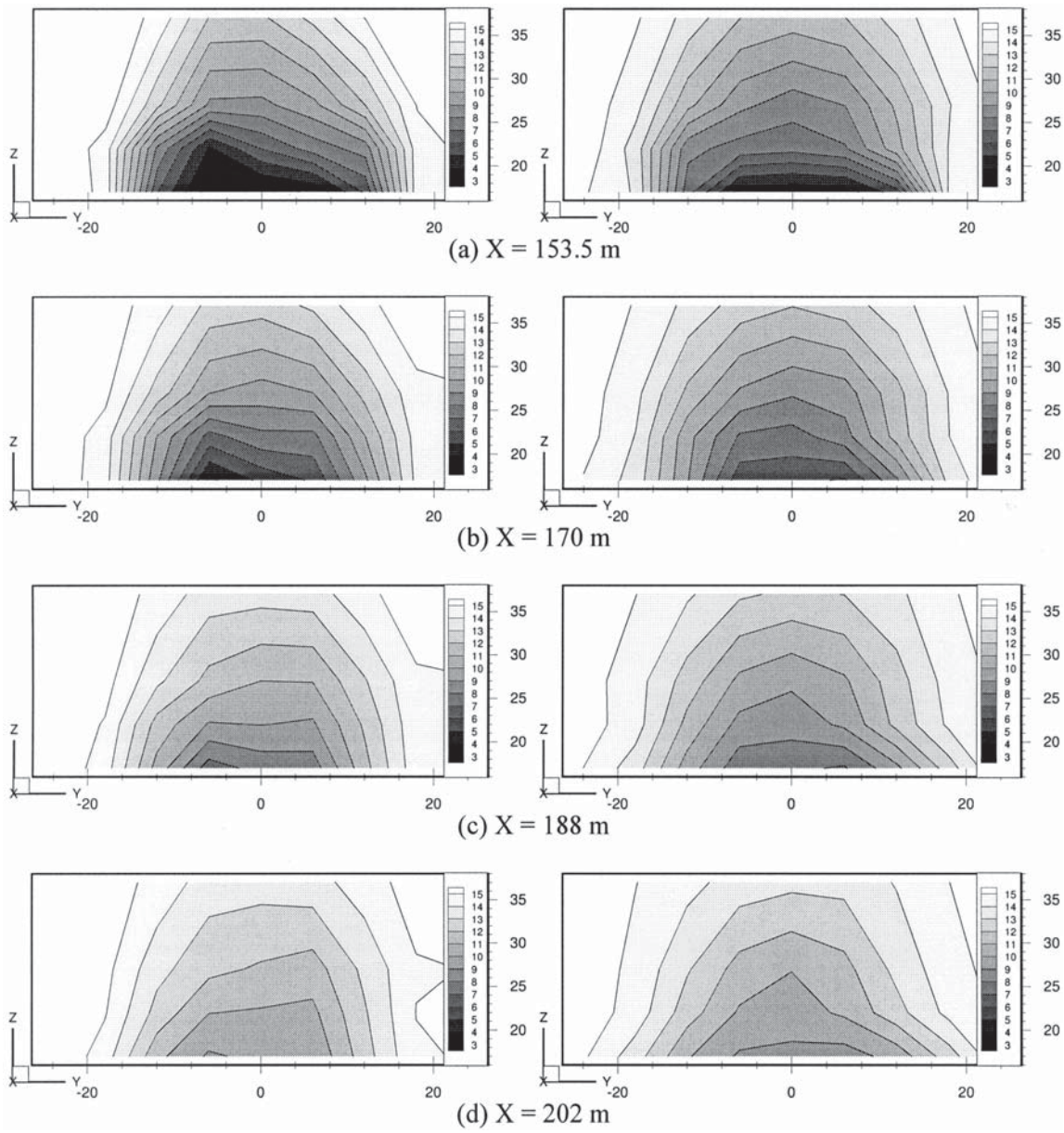

Fig. 18 A comparison of the time-averaged velocity magnitude (m/s) between the experiments and the computed solution for WOD = 0 at different Y–Z planes on the deck of the LPD-17 ship. Experimental results are on the left and the simulation results are on the right

Figure 18 compares the time-averaged velocity magnitude from experiments and simulations at different Y–Z planes on the deck of the LPD-17 ship. The experiments were conducted in a wind tunnel on a 1/94th scale model [**15**]. A reasonable match is obtained between the experimental and the numerical results. The wake in the experiments appears to be larger and more asymmetric than that obtained in the simulations. This could be due to the inviscid flow assumption used for the simulations. The simulations do not capture the boundary layer on the ship surface ahead of the hangar; the width of this boundary layer contributes to the wake on the ship deck. However, the differences are very small and a good overall match is observed.

4 CONCLUSIONS

This article provides a detailed literature review of previous work in the areas of dynamic interface, blade sailing, and ship airwake. Both steady and time-accurate inviscid CFD simulations of the airwake of two different classes of ships, LHA and LPD-17, were performed and presented. The parallel, finite-volume flow solver, PUMA2, was used with unstructured grids on full-scale models.

The CFD results, which are presented in this article, showed significant time-varying flow effects over the selected landing spots. The time accurate results show significant temporal and spatial variation that may be responsible for additional pilot workload. A good comparison with experimentally observed velocity field over the LPD-17 deck is obtained. In addition, a general agreement of the dominant shedding frequencies for LHA simulations with previous results is observed.

REFERENCES

1 **Lee, D., Sezer-Uzol, N., Horn, J. F.,** and **Long, L. N.** Simulation of helicopter shipboard launch and recovery with time-accurate airwakes. AHS 59th Annual Forum, Phoenix, AZ, 6–8 May 2003.

2 **Lee, D., Horn, J. F., Sezer-Uzol, N.,** and **Long, L. N.** Simulation of pilot control activity during helicopter shipboard operation. AIAA Atmospheric Flight Mechanics Conference and Exhibit, Austin, TX, 11–14 August 2003, AIAA paper 2003-5306.

3 **Lee, D., Sezer-Uzol, N., Horn, J. F.,** and **Long, L. N.** Simulation of helicopter shipboard launch and recovery with time-accurate airwakes. *J. Aircraft*, 2005, **42**(2), 448–461.

4 **Wilkinson, C. H., Zan, S. J., Gilbert, N. E.,** and **Funk, J. D.** Modelling and simulation of ship air wakes for helicopter operations – a collaborative venture. NATO RTO Applied Vehicle Technology Panel (AVT) Symposium on *Fluid Dynamics Problems of Vehicles Operating Near or in the Air-Sea Interface*, Amsterdam, The Netherlands, 5–8 October 1998.

5 **Wilkinson, C. H., Roscoe, M. F.,** and **VanderVliet, G. M.** Determining fidelity standards for the shipboard launch and recovery task. AIAA Modeling and Simulation Technologies Conference and Exhibit, Montreal, Canada, 6–9 August 2001, AIAA paper 2001–4062.

6 **Polsky, S. A.** and **Bruner, C. W. S.** Time-accurate computational simulations of an LHA ship airwake. 18th AIAA Applied Aerodynamics Conference, Denver, CO, 14–17 August 2000, AIAA paper 2000-4126.

7 **Polsky, S. A.** A computational study of unsteady ship airwake. 40th AIAA Aerospace Sciences Meeting and Exhibit, Reno, Nevada, 14–17 January 2002, AIAA paper 2002-1022.

8 **Daley, W. H.** *Flow visualization of the airwake around a model of a TARAWA class LHA in a simulated atmospheric boundary layer*. MS Thesis, Department of Aeronautical Engineering, Naval Postgraduate School, Monterey, CA, 1988.

9 **Johns, M. K.** *Flow visualization of the airwake around a model of a DD-963 class destroyer in a simulated atmospheric boundary layer*. MS Thesis, Department of Aeronautical Engineering, Naval Postgraduate School, Monterey, CA, 1988.

10 **Johns, M. K.** and **Healey, J. V.** The airwake of a DD-963 class destroyer. *Naval Engrs J.*, 1989, **101**(3), 36–42.

11 **Healey, J. V.** A data base for flight in the wake of a ship. 30th AIAA Aerospace Sciences Meeting and Exhibit, Reno, NV, 6–9 January 1992.

12 **Healey, J. V.** Establishing a database for flight in the wakes of structures. *J. Aircraft*, 1992, **29**(4), 559–564.

13 **Rhodes, M. M.** and **Healey, J. V.** Flight deck aerodynamics of a nonaviation ship. *J. Aircraft*, 1992, **29**(4), 619–626.

14 **Tai, T. C.** Simulation of LPD ship airwake by Navier–Stokes method. In Proceedings of the Sixth Asian Congress of Fluid Mechanics, Singapore, May 1995.

15 **Guillot, M. J.** and **Walker, M. A.** Unsteady Analysis of the Air Wake over the LPD-17. 18th AIAA Applied Aerodynamics Conference and Exhibit, Denver, CO, 14–17 August 2000, AIAA paper 2000–4125.

16 **Zan, S. J.** and **Garry, E. A.** *Wind tunnel measurements of the airwake behind a model of a generic frigate*. NRC-CNRC report LTR-AA-13, 1994.

17 **Zan, S. J., Syms, G. F.,** and **Cheney, B. T.** Analysis of patrol frigate air wakes, In Proceedings of the NATO RTO Symposium on *Fluid Dynamics Problems of Vehicles Operating near or in the Air–Sea Interface*, Amsterdam, The Netherlands, 5–8 October 1998.

18 **Syms, G. F.** Numerical simulation of frigate airwakes. *Int. J. Comput. Fluid Dyn.*, 2004, **18**(2), 199–207.

19 **Cheney, B. T.** and **Zan, S. J.** *CFD code validation data and flow topology for the technical co-operation program AER-TP2 simple frigate shape*. NRC-CNRC report LTR-A-035, National Research Council Canada Institute for Aerospace Research, 1999.

20 **Zan, S. J.** Surface flow topology for a simple frigate shape. *Can. Aeronaut. Space J.*, 2001, **47**(1), 33–43.

21 **Taghizad, A., Verbeke, C.,** and **Desopper, A.** Aerodynamic perturbations encountered by a helicopter landing on a ship – effects on the helicopter flight

dynamics. NATO RTO Applied Vehicle Technology Panel (AVT) Symposium on *Fluid Dynamics Problems of Vehicles Operating Near or in the Air–Sea Interface*, Amsterdam, The Netherlands, 5–8 October 1998.

22 **Maslov, L. A., Valuev, N. D.,** and **Zharinov, A. V.** The experience of aerodynamic disturbances research behind an aircraft-carrier ship with elements for safe operation of ship-based aircraft. NATO RTO Applied Vehicle Technology Panel (AVT) Symposium on Fluid *Dynamics Problems of Vehicles Operating Near or in the Air–Sea Interface*, Amsterdam, The Netherlands, 5–8 October 1998.

23 **Ball, J. C.** XV-15 shipboard evaluation. 39th AHS Annual Forum, 9–11 May 1983.

24 **Ball, J. C.** and **White, W. R.** *H-46 dynamic interface tests aboard USS GUAM (LPH-9)*. NAVAIRTESTCEN Technical report RW-28R-83, 1984.

25 **Williams, S. L.** and **Long, K. R.** Dynamic interface flight tests and the pilot rating scale. AHS 53rd Annual Forum, Virginia Beach, VA, 29 April–1 May 1997.

26 **Zan, S. J.** Experimental determination of rotor thrust in a ship airwake. *J. Am. Helicopter Soc.*, 2002, **47**(2), 100–114.

27 **Lee, R. G.** and **Zan, S. J.** Unsteady aerodynamic loading on a helicopter fuselage in a ship airwake. *J. Am. Helicopter Soc.*, 2004, **49**(2), 149–159.

28 **Silva, M. J., Yamauchi, G. K., Wadcock, A. J.,** and **Long, K. R.** Wind tunnel investiagation of the aerodynamic interactions between helicopters and tiltrotors in a shipboard environment. Presented at the American Helicopter Society 4th Decennial Specialist's Conference on *Aeromechanics*, San Francisco, CA, 21–23, January 2004.

29 **Silva, M. J., Geyer, W. P., Nelson, J.,** and **Mason, D. H.** Full-Scale rotorcraft downwash surveys in a shipboard environment. AHS 60th Annual Forum, 7–10 June 2004.

30 **Tai, T. C.** and **Carico, D.** Simulation of DD-963 ship airwake by Navier-Stokes method. 24th AIAA Fluid Dynamics Conference, Orlando, FL, 6–9 July 1993, AIAA paper 93-3002. *J. Aircraft*, 1995, **32**(6), 1399–1401.

31 **Tai, T. C.** Simulation and analysis of LHD ship airwake by Navier–Stokes method. NATO RTO Applied Vehicle Technology Panel (AVT) Symposium on *Fluid Dynamics Problems of Vehicles Operating Near or in the Air-Sea Interface*, Amsterdam, The Netherlands, 5–8 October 1998.

32 **Reddy, K. R., Toffoletto, R.,** and **Jones, K. R. W.** Numerical simulation of ship airwake. The Computational Techniques and Applications Conference, Adelaide, Australia, 29 September–1 October 1997. *Comput. Fluids*, 2000, **129**, 451–465.

33 **Moctar, O. E.** and **Bertram, V.** Computation of viscous flow around fast ship superstructures. Twenty-Fourth Symposium on *Naval Hydrodynamics*, Fukuoka, Japan, 8–13 July 2003.

34 **Bogstad, M. C., Habashi, W. G., Akel, I., Ait-Ali-Yahia, D., Giannias, N.,** and **Longo, V.** Computational-fluid-dynamics based advanced ship-airwake database for helicopter flight simulators. *J. Aircraft*, 2002, **39**(5), 830–838.

35 **Zan, S. J.** Technical comment on 'Computational-fluid-dynamics based advanced ship-airwake database for helicopter flight simulation'. *J. Aircraft*, 2003, **40**(5), 1007.

36 **Landsberg, A. M., Sandberg, W. C., Young, T. R., Jr,** and **Boris, J. P.** *DDG-51 Flt-IIA airwake study. Part 2. Hangar interior flow*. NRL/MR/6410-96-7898. Laboratory for Computational Physics and Fluid Dynamics, Naval Research Laboratory, Center for Reactive Flow and Dynamical Systems, 1996.

37 **Camelli, F. E., Soto, O., Lohner, R., Sandberg, W. C.,** and **Ramamurti, R.** Topside LPD17 flow and temperature study with an implicit monolithic scheme. 41st AIAA Aerospace Sciences Meeting & Exhibit, Reno, Nevada, 6–9 January 2003, AIAA paper 2003-0969.

38 **Camelli, F., Lohner, R., Sandberg, W.,** and **Ramamurti, R.** VLES study of ship stack gas dynamics. 42nd AIAA Aerospace Sciences Meeting and Exhibit, Reno, NV, 5–8 January 2004, AIAA paper 2004-72.

39 **Polsky, S. A.** CFD Prediction of airwake flowfields for ships experiencing beam winds. 21st AIAA Applied Aerodynamics Conference, 2003, AIAA paper 2003-3657.

40 **Arunajatesan, S., Shipman, J. D.,** and **Sinha, N.** Towards numerical modeling of coupled VSTOL-ship airwake flowfields. 42nd AIAA Aerospace Sciences Meeting and Exhibit, Reno, NV, 5–8 January 2004, AIAA paper 2004-0052.

41 **Arunajatesan, S., Shipman, J.,** and **Sinha, N.** Numerical modeling of coupled VSTOL-ship airwake flowfields. HT-FED04-56147, Proceedings of HT-FED04, 2004 ASME Heat Transfer/Fluids Engineering Summer Conference, Charlotte, NC, 25–29 July 2004, pp. 323–333.

42 **Zan, S. J.** and **Syms, G. F.** Numerical prediction of rotor loads in an experimentally-determined ship airwake. Report LTR-AA-15. National Research Council of Canada, Ottawa, Ontario, Canada, 1995.

43 **Landsberg, A. M., Young, T. R., Jr,** and **Boris, J. P.** Analysis of the nonlinear coupling effects of a helicopter downwash with an unsteady ship airwake. 33rd AIAA Aerospace Sciences Meeting and Exhibit, Reno, NV, 9–12 January 1995, AIAA paper 95-0047.

44 **Tattersall, P., Albone, C. M., Soliman, M. M.,** and **Allen, C. B.** Prediction of ship air wakes over flight decks using CFD. NATO RTO Applied Vehicle Technology Panel (AVT) Symposium on *Fluid Dynamics Problems of Vehicles Operating Near or in the Air–Sea Interface*, Amsterdam, The Netherlands, 5–8 October 1998.

45 **Wakefield, N. H., Newman, S. J.,** and **Wilson, P. A.** Helicopter flight around a ship's structure. *Proc. Instn Mech. Engrs, Part G: J. Aerospace Engineering*, 2002, **216**(G1), 13–28.

46 **Liu, J.** and **Long, L. N.** Higher order accurate ship airwake predictions for the helicopter-ship interface problem. AHS 54th Annual Forum, Washington DC, 20–22 May 1998.

47 **Long, L. N., Liu, J.,** and **Modi, A.** Higher order accurate solutions of ship airwake flow fields using parallel computers. NATO RTO Applied Vehicle Technology Panel (AVT) Symposium on *Fluid Dynamics Problems of Vehicles Operating Near or in the Air-Sea Interface*, Amsterdam, The Netherlands, 5–8 October 1998.

48 **Modi, A.** *Unsteady separated flow simulations using a cluster of workstations*. MS Thesis, Department of

Aerospace Engineering, The Pennsylvania State University, 1999.

49 **Sharma, A.** and **Long, L. N.** Airwake simulations on an LPD 17 Ship. 15th AIAA Computational Fluid Dynamics Conference, Anaheim, California, 11–14 June 2001, AIAA paper 2001–2589.

50 **Sharma, A.** *Parallel methods for unsteady, separated flows and aerodynamic noise prediction*. MS Thesis, Department of Aerospace Engineering, The Pennsylvania State University, 2001.

51 **Hurley, G. E., Pittman, C. W.,** and **Trick, L. L.** *HH-46E/CV-64 rotor engage/disengage test*. NAVAIRTESTCEN report of test results RW-55R-84, 1984.

52 **Hurst, D. W.** and **Newman, S. J.** Wind tunnel measurements of ship induced turbulence and the prediction of helicopter rotor blade response. 11th European Rotorcraft Forum, London, England, 10–13 September 1985, paper no. 99.

53 **Newman, S. J.** *Second blade sailing wind tunnel test*. Report AASU 93/1. Department of Aeronautics and Astronautics, University of Southampton, 1993.

54 **Newman, S. J.** The problems of rotor engagement and diengagement of a shipborne helicopter. *J. Naval Sci.*, 1994, **20**(1), 56.

55 **Newman, S. J.** The verification of a theoretical helicopter rotor blade sailing method by means of wind tunnel testing. *Aeronaut. J. R. Aeronaut. Soc.*, 1995, **99**(982), 41–51.

56 **Newman, S. J.** A theoretical model for predicting the blade sailing behaviour of a semi-rigid rotor helicopter. *Vertica*, 1990, **14**(4), 531–544.

57 **Newman, S. J.** *An investigation into the phenomenon of helicopter blade sailing (rotors)*. PhD Thesis, University Of Southampton (UK), 1995.

58 **Newman, S. J.** and **Walker, W. R.** The Influence of blade flexibility on the sailing behaviour of helicopter rotors. *J. Defence Sci.*, 1996, **4**, 498.

59 **Newman, S. J.** The phenomenon of helicopter rotor blade sailing. *Proc. Instn Mech. Engrs*, 1999, **213**, 347– 363.

60 **Newman, S. J.** The design, development and operation of the shipborne helicopter, *Trans. R. Instn Naval Architects*, 1999, **141**(C), 192–210.

61 **Geyer, W. P., Jr**. and **Smith, E. C.** Aeroelastic analysis of transient blade dynamics during shipboard engage/disengage operations. AHS, International Aeromechanics Specialists' Conference, Second Aeromechanics Technology and Product Design for the 21st Century, Proceedings, Bridgeport, CT, 11–13 October 1995, Vol. 2, pp. 8-91–8-114.

62 **Geyer, W. G., Keller, J.,** and **Smith, E. C.** Validation and application of a transient response analysis for shipboard engage/disengage operations. AHS 52nd Annual Forum, Washington, DC, 4–6 June 1996.

63 **Kang, H.** and **Smith, E. C.** Transient response analysis of gimballed tiltrotors during engage and disengage operations. 39th AIAA/ASME/ASCE/AHS/ASC Structures, Structural Dynamics, and Materials Conference, Long Beach, CA, 20–23 April 1998.

64 **Smith, E. C., Keller, J. A.,** and **Kang, H.** Recent developments in the analytical investigation of shipboard rotorcraft engage and disengage operations. NATO RTO Applied Vehicle Technology Panel (AVT) Symposium on *Fluid Dynamics Problems of Vehicles Operating Near or in the Air-Sea Interface*, Amsterdam, The Netherlands, 5–8 October 1998.

65 **Keller, J. A.** and **Smith, E. C.** Analysis and control of the transient shipboard engagement behavior of rotor systems. AHS 55th Annual Forum, Montreal, Quebec, Canada, 25–27 May 1999.

66 **Keller, J. A.** and **Smith, E. C.** Experimental and theoretical correlation of helicopter rotor blade-droop stop impacts. *J. Aircraft*, 1999, **36**(2), 443–450.

67 **Keller, J. A.** *Analysis and control of the transient aeroelastic response of rotors during shipboard engagement and disengagement operations*. PhD Thesis, Department of Aerospace Engineering, The Pennsylvania State University, 2001.

68 **Keller, J. A.** and **Smith, E. C.** Active control of gimballed rotors using swashplate actuation during shipboard engagement operations, *J. Aircraft*, 2003, **40**(4), 726–733.

69 **Kang, H., He, C.,** and **Carico, D.** Modeling and simulation of rotor engagement/disengagement in shipboard operation. AHS 60th Annual Forum, Baltimore, MD, 7–10 June 2004.

70 **Healey, J. V.** The prospects for simulating the helicopter/ship interface. *Naval Engrs J.*, 1987, **99**(2), 45–63.

71 **Tate, S. J.** and **Padfield, G. D.** Simulating flying qualities at the helicopter/ship dynamic interface. *AHS 50th Annual Forum*, Washington, DC, 11–13 May 1994.

72 **Williams, S.** and **Long, K.** The US NAVY's use of visual simulation technology to optimize and refine shipboard rotorcraft compatibility. AHS 53rd Annual Forum, Virginia Beach, Virginia, 29 April –1 May 1997.

73 **Lumsden, B. R., Wilkinson, C. H.,** and **Padfield, G. D.** Challanges at the helicopter–ship dynamic interface. 24 th European Rotorcraft Forum, Marseilles, France, 15–17 September 1998.

74 **de Ferrier, B.** and **Langlois, B.** Simulation tools in the calculation of aircraft-ship interface operational limits. NATO RTO Applied Vehicle Technology Panel (AVT) Symposium on *Fluid Dynamics Problems of Vehicles Operating Near or in the Air-Sea Interface*, Amsterdam, The Netherlands, 5–8 October 1998.

75 **Wilkinson, C. H., VanderVliet, G. M.,** and **Roscoe, M. F.** Modeling and simulation of the ship-helicopter environment. AIAA Modeling and Simulation Technologies Conference and Exhibit, Denver, CO, 14–17 August 2000, AIAA paper 2000-4583.

76 **Bunnell, J. W.** An integrated time-varying airwake in a UH-60 black hawk shipboard landing simulation. AIAA Modeling and Simulation Technologies Conference and Exhibit, Montreal, Canada, 6–9 August 2001, AIAA paper 2001-4065.

77 **Lee, D.** and **Horn, J. F.** Simulation and control of helicopter shipboard launch and recovery operations. AHS Flight Controls and Crew System Design Specialists' Meeting, Philadelphia, PA, 9–11 October 2002.

78 **VanderVliet, G. M., Wilkinson, C. H.,** and **Roscoe, M. F.** Verification, validation, and accreditation of a flight simulator: the JSHIP experience. AIAA Modeling and Simulation Technologies Conference and Exhibit, Montreal, Canada, 6–9 August 2001, AIAA paper 2001-4061.

79 **Roscoe, M. F.** and **Wilkinson, C. H.** DIMSS-JSHIP'S modeling and simulation process for ship/helicopter testing and training. AIAA Modeling and Simulation Technologies Conference and Exhibit, Monterey, CA, 5–8 August 2002, AIAA paper 2002-4597.

80 **Xin, H.** and **He, C.** A combined technique for inverse simulation applied to rotorcraft shipboard operations. AHS 58th Annual Forum, Montreal, Canada, 11–13 June 2002.

81 **Roscoe, M. F.** and **Thompson, J. H.** JSHIP's dynamic interface modeling and simulation system: a simulation of the UH-60A helicopter/LHA shipboard environment task. AHS 59th Annual Forum, Phoenix, AZ, 6–8 May 2003.

82 **McKillip, R. J., Boschitsch, A., Quackenbush, T., Keller, J.,** and **Wachspress, D.** Dynamic interface simulation using a coupled vortex-based ship airwake and rotor wake model. AHS 58th Annual Forum, Montreal, Canada, 11–13 June 2002.

83 **He, C., Xin, H.,** and **Bhagwat, M.** Advanced rotor wake interface modeling for multiple rotorcraft shipboard landing simulation. AHS 59th Annual Forum, Baltimore, MD, 7–10 June 2004.

84 **Bruner, C. W. S.** *Parallelization of the Euler equations on unstructured grids*. PhD Dissertation, Virginia Polytechnic Institute and State University, 1996.

85 **Modi, A., Sezer-Uzol, N., Long, L. N.,** and **Plassmann, P. E.** Scalable computational steering system for visualization of large-scale CFD simulations. 32nd AIAA Fluid Dynamics Conference and Exhibit, St. Louis, Missouri, 24–27, June 2002, AIAA paper 2002-2750.

86 **Modi, A., Sezer-Uzol, N., Long, L. N.,** and **Plassmann, P. E.** Scalable computational steering for visualization and control of large-scale fluid dynamics simulations. *J. Aircraft*, 2005, **42**(4), 963–975.

87 **Souliez, F. J.** *Parallel methods for the computation of unsteady separated flows around complex geometries*. PhD Thesis, Department of Aerospace Engineering, The Pennsylvania State University, 2002.

88 **Jindal, S., Long, L. N., Plassmann, P. E.,** and **Sezer-Uzol, N.** Large eddy simulations on a sphere using unstructured grids. 34th AIAA Fluid Dynamics Conference and Exhibit, Portland, OR, 28 June –1 July 2004.

89 *Gridgen* (Pointwise, Inc., http://pointwise.com), 2005.

90 **Long, L. N., Plassmann, P. E., Sezer-Uzol, N.,** and **Jindal, S.** Real-time visualization and steering of large-scale parallel simulations. 11th International Symposium on Flow Visualization, University of Notre Dame, Notre Dame, IN, 9–12 August 2004.

APPENDIX 1

Notation

CFD	Computational Fluid Dynamics
CFL	Courant-Friedrichs-Lewy
COCOA3	Cost effective Computing Array-3
DI	Dynamic Interface
FAST3D	a CFD flow solver
LCAC	Landing Craft Air Cushion
LCU	Landing Craft Utility
LES	Large Eddy Simulations
MILES	Monotone Integrated Large Eddy Simulation
MPI	Message Passing Interface
NLDE	Non-Linear Disturbance Equations
POSSE	Portable Object-oriented Scientific Steering Environment
PSD	Power Spectral Density
PUMA	Parallel Unstructured Maritime Aerodynamics
RAM	Random Access Memory
RANS	Reynolds Averaged Navier-Stokes
RW	Rotary Wing aircraft
SHOLs	Safe Helicopter Operating Limits
SOR	Successive Over-Relaxation Schemes
SST	Shear Stress Transport
STOVL	Short Take Off Vertical Landing
VTOL	Vertical Take Off and Landing
V/STOL	Vertical/Short Take Off and Landing
WOD	Wind-Over-the-Deck

Ships

CPF	Canadian Patrol Frigate
CVN-75	an aircraft carrier
DDG-51 Flt-IIA	a SPRUANCE class destroyer
DD-963	a SPRUANCE class destroyer
GF	Generic Frigate
LHA	Landing Helicopter Assault
LPD	Landing Platform Dock
LHD	Landing Helicopter Deck
LPH	Landing Platform Helicopter
SFS	Simple Frigate Shape
SES	Surface Effect Ship

Aircraft

AH-1	Super Cobra helicopter
AV-8B	Harrier
CH-46	Sea Knight helicopter
CH-53	Sea Stallion helicopter
CH-53E	Super Stallion helicopter
F-35	Joint Strike Fighter (JSF)
H-46	Sea Knight helicopter
MV22	Osprey tiltrotor
UH-1	Huey helicopter
UH-60A	Black Hawk helicopter
XP-15	tiltrotor

APPENDIX 2

A few details of the Tarawa LHA class ship are as follows (see http://www.chinfo.navy.mil/ for additional information).

1. Builders: Ingalls Shipbuilding, Pascagoula, Ms.
2. Power plant: two boilers, two geared steam turbines, two shafts, 70 000 total shaft horsepower.
3. Length: 820 ft (249.9 ms).
4. Beam: 106 ft (31.8 m).
5. Displacement: 39 400 tons (40 032 metric tons) full load.
6. Speed: 24 knot (27.6 miles/h).
7. Aircraft, depending on mission: 12 CH-46 Sea Knight helicopters, four CH-53E Sea Stallion helicopters, six AV-8B Harrier attack aircraft, three UH-1 N Huey helicopters, four AH-1W Super Cobra helicopters.
8. Ships
   (a) USS Tarawa (LHA 1), San Diego, CA;
   (b) USS Saipan (LHA 2), Norfolk, VA;
   (c) USS Belleau Wood (LHA 3), San Diego, CA;
   (d) USS Nassau (LHA 4), Norfolk, VA;
   (e) USS Peleliu (LHA 5), San Diego, CA.
9. Crew: ship company–82 officers, 882 enlisted, Marine Detachment 1900 plus.
10. Armament: two RAM launchers, two Phalanx 20 mm CIWS mount, three 500. cal. machine guns, four 25 mm Mk 38 machine guns.
11. Date deployed: 29 May, 1976 (USS Tarawa).

A few details of the San Antonio LPD class ship are as folows (see http://www.chinfo.navy.mil/ for additional information).

1. Builders: Northrop Grumman Ships Systems, with Raytheon Systems Corporation and Intergraph Corporation.
2. Power plant: four sequentially turbocharged marine Colt-Pielstick diesels, two shafts, 41 600 shaft horsepower.
3. Length: 684 ft (208.5 ms).
4. Beam: 105 ft (31.9 m).
5. Displacement: approximately 24 900 tons (25 300 metric tons) full load.
6. Speed: in excess of 22 knot (24.2 mile/h, 38.7 km/h).
7. Aircraft: launch or land two CH53E Super Stallion helicopters or up to four CH-46 Sea Knight helicopters, MV22-Osprey tiltrotor aircraft, AH-1, or UH-1 helicopters.
8. Armament: two Bushmaster II 30 mm close in guns, fore and aft; two rolling airframe missile launchers, fore, and aft.
9. Landing craft/assault vehicles: two landing craft air cushions or one landing craft utility, and 14 advanced amphibious assault vehicles.
10. Ships
    (a) San Antonio (LPD 17);
    (b) New Orleans (LPD 18);
    (c) Mesa Verde (LPD 19);
    (d) Green Bay (LPD 20);
    (e) New York (LPD 21).
11. Crew: ship company – 361 (28 officers, 333 enlisted; embarked landing force – 699 (66 officers, 633 enlisted); surge capacity to 800.